おおざっぱな現状の位置づけ

- ☑単分子の電気抵抗を測れるか？
- ☑定性的な伝導特性の解釈はできるか？
- □定量的な解釈はできるか？
- ☑外部変調は可能か？
- ☑整流特性は出るか？
- ☑分子の個性／機能は出せるか？

- □評価方法としてつかえるか？

分子接合の電気伝導度を決める要因

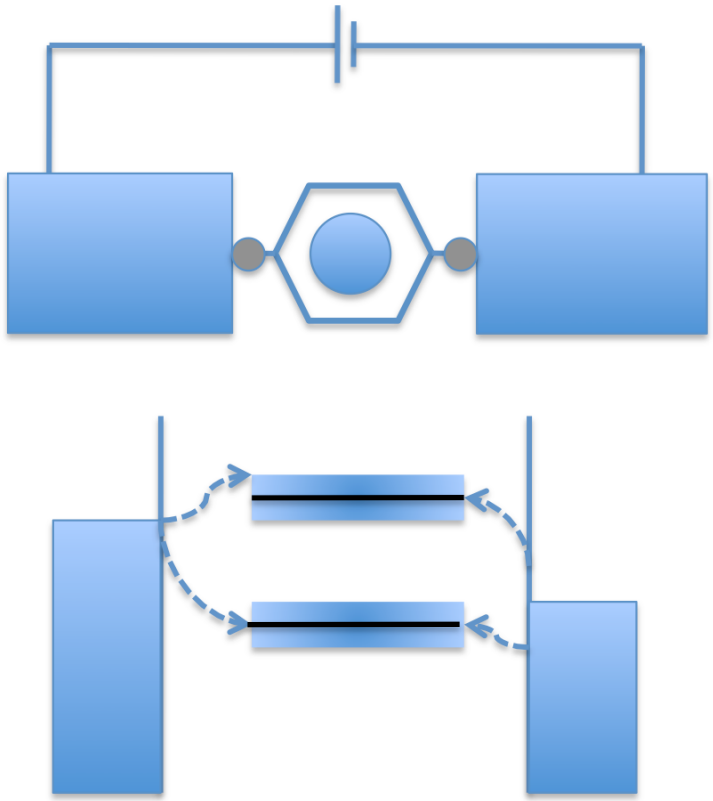

・電極との電子カップリングにより分子軌道が広がる。
・広がりの幅はコンタクト部分の設計により調整可能。

1. 分子の電子状態

2. 分子／電極のカップリングの強さ

期待される輸送特性

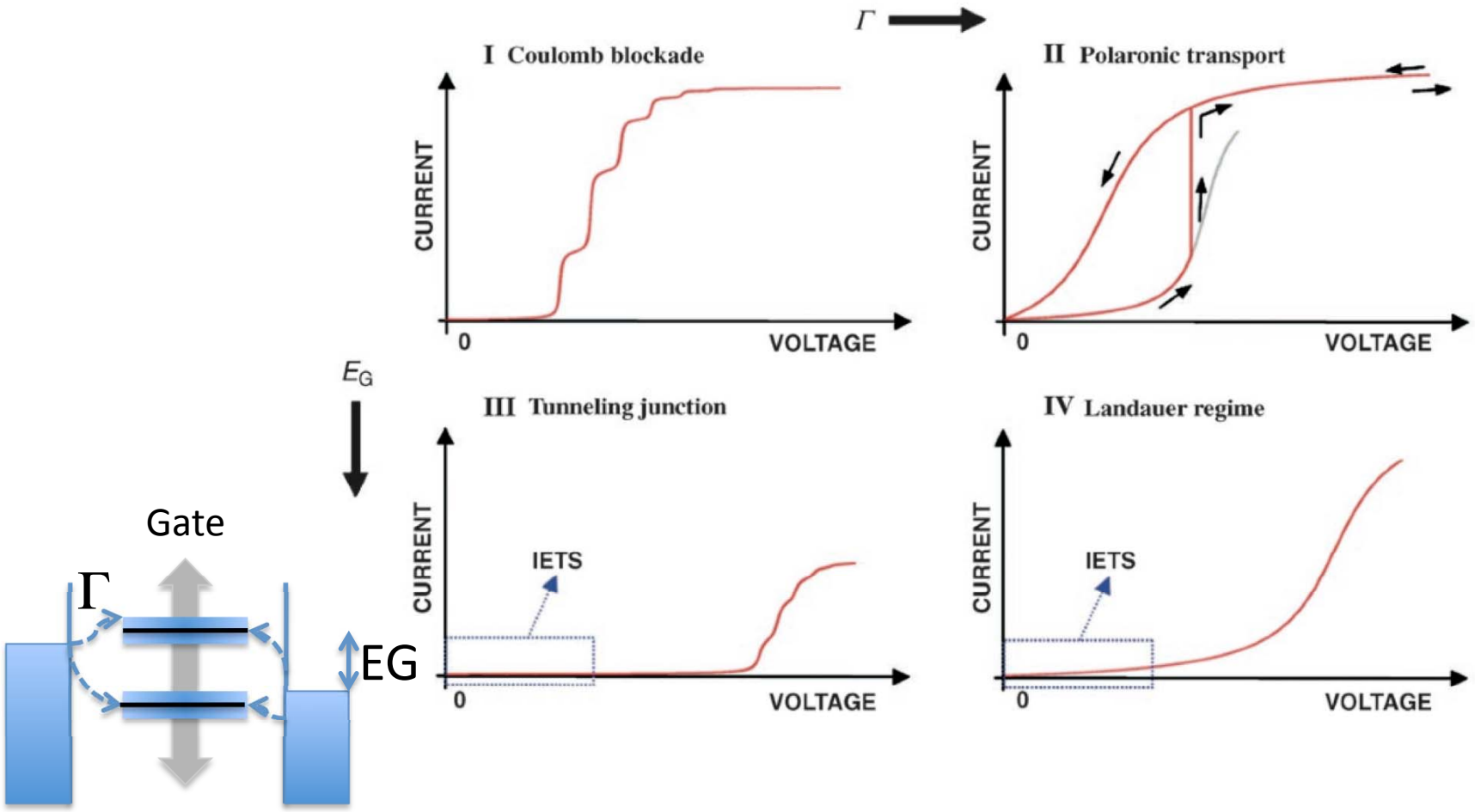

Troisi and Ratner, small, 2, 172, 2006.

単分子接合研究（計測）の状況

1974 単分子整流器の提言（Aviram, Ratner）

1997 単分子電気伝導度測定の報告（Reed@USA）

2001 Schönによる単分子FETの報告 → ウソ

2001 911テロ: Nanotechnology から National Securityへ

2002 単分子によるクーロンブロッケードおよび近藤効果@USA

→ 2005 分子を入れなくても同じ現象が観測できる！

2002 水素分子の電気伝導度計測（オランダ）

2003 定量的な評価方法の確立（USA）

2006 分子構造依存などの詳細な検討(USA)

2008 安定な分子接合の構築に成功(ドイツ)

2009 分子ダイオード特性の計測に成功（USA）

黎明期

混乱期

復活の兆し

初めての計測例

Conductance of a Molecular Junction

M. A. Reed,* C. Zhou, C. J. Muller, T. P. Burgin, J. M. Tour*

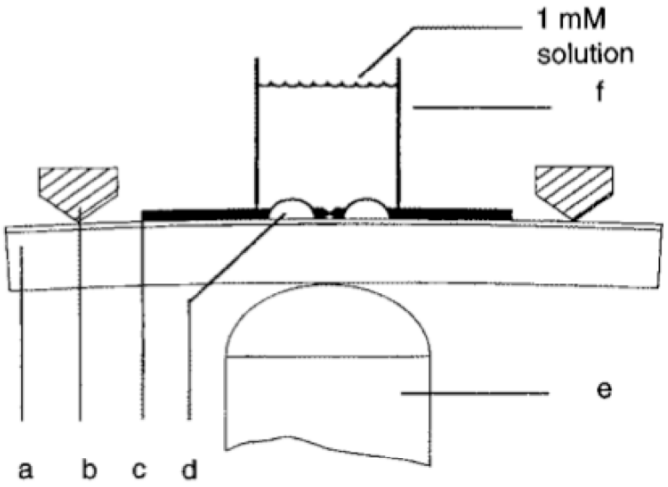

Fig. 1. A schematic of the MCB junction with (a) the bending beam, (b) the counter supports, (c) the notched gold wire, (d) the glue contacts, (e) the pizeo element, and (f) the glass tube containing the solution.

SCIENCE • VOL. 278 • 10 OCTOBER 1997 •

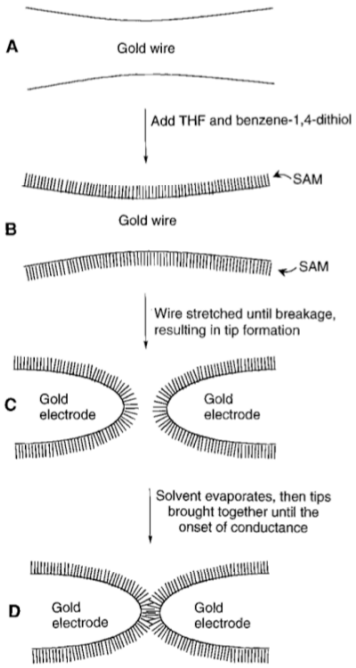

Fig. 2. Schematic of the measurement process. (**A**) The gold wire of the break junction before breaking and tip formation. (**B**) After addition of benzene-1,4-dithiol, SAMs form on the gold wire surfaces. (**C**) Mechanical breakage of the wire in solution produces two opposing gold contacts that are SAM-covered. (**D**) After the solvent is evaporated, the gold contacts are slowly moved together until the onset of conductance is achieved. Steps (C) and (D) (without solution) can be repeated numerous times to test for reprodicibility.

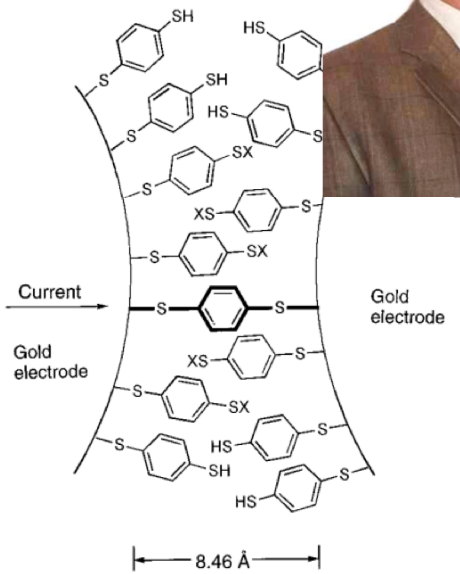

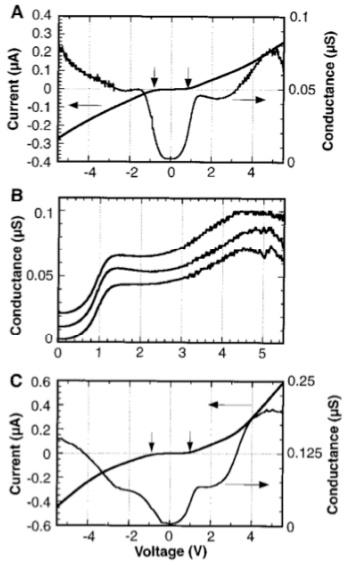

電極構造

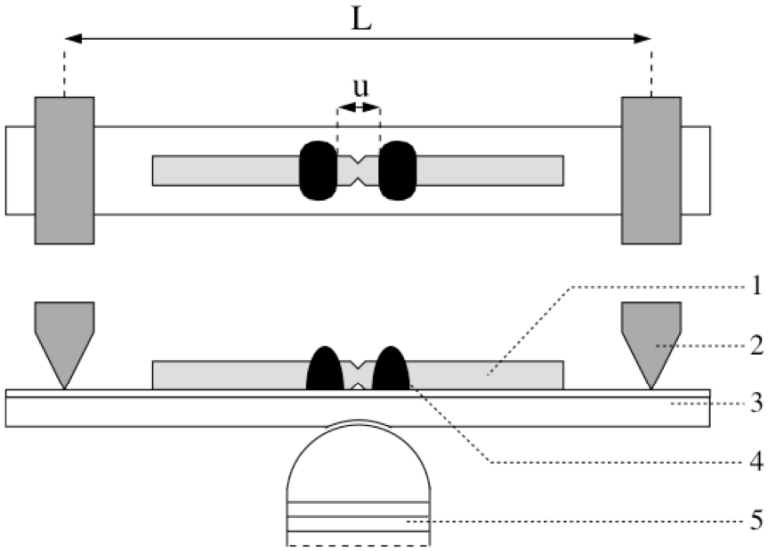

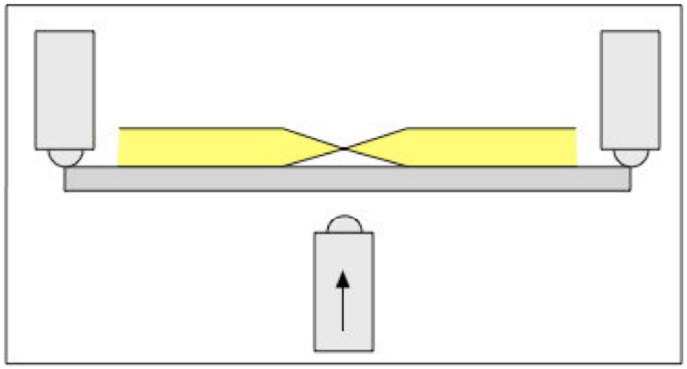

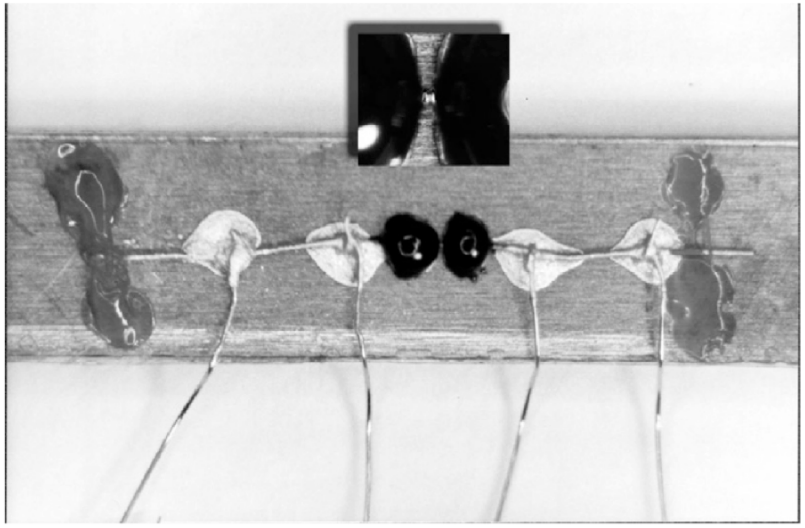

N. Agraït et al. / Physics Reports 377 (2003) 81–279

Mechanically Controllable Break Junction (MCBJ) / J. van Ruitenbeek

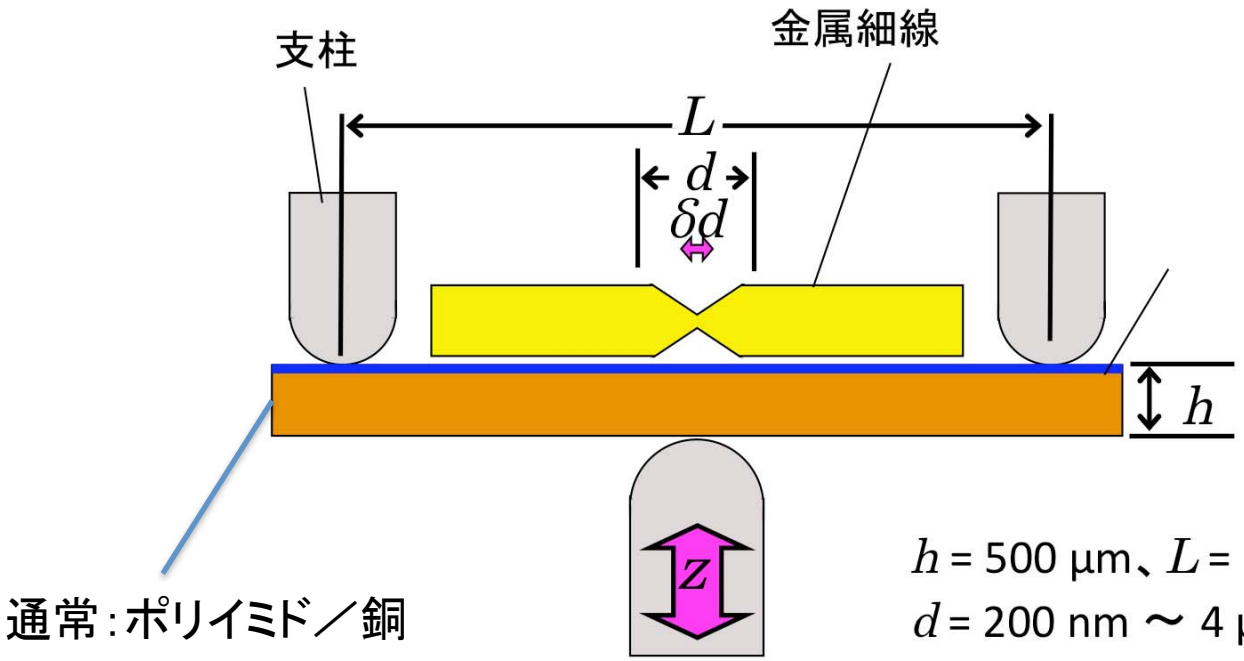

$$\frac{\delta d}{z} = \frac{6dh}{L^2} < \frac{1}{10000}$$

分子機能を出した例+より精密な測定例

PR-B 59, 12505, 1999.

Electron transport through a metal-molecule-metal junction

C. Kergueris, J.-P. Bourgoin,* and S. Palacin
Service de Chimie Moléculaire, CEA-Saclay, 91191 Gif-sur-Yvette Cedex, France

D. Esteve and C. Urbina
Service de Physique de l'Etat Condensé, CEA-Saclay, 91191 Gif-sur-Yvette Cedex, France

M. Magoga and C. Joachim
CEMES-CNRS, BP4347, 31055 Toulouse Cedex, France
(Received 17 November 1998)

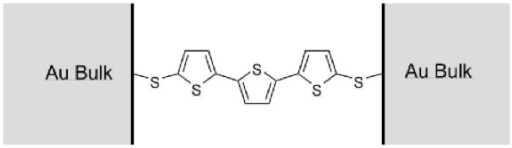

FIG. 1. Ideal sample. A conjugated molecule is chemisorbed onto the gold electrodes via the thiolate terminal groups.

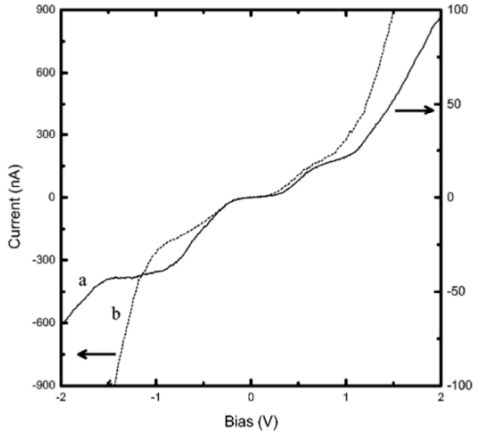

FIG. 7. Typical (a) asymmetric (solid line) and (b) symmetric (dashed line) *I-V* curves recorded at room temperature for gold-*T*3-gold junctions. Both curves were obtained by averaging over five voltage sweeps.

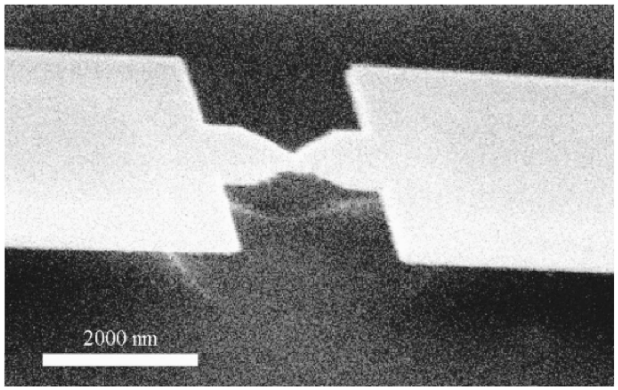

FIG. 3. Scanning electron microscope picture of a suspended junction before breaking.

精密なMCBJ

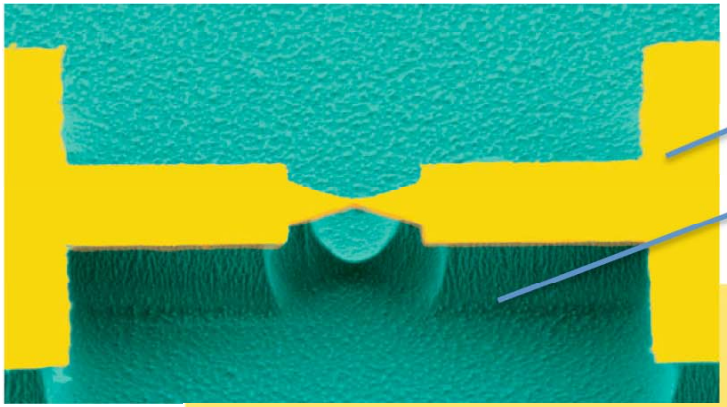

電極

ポリイミド（絶縁膜）

りんせい銅（バネ材）

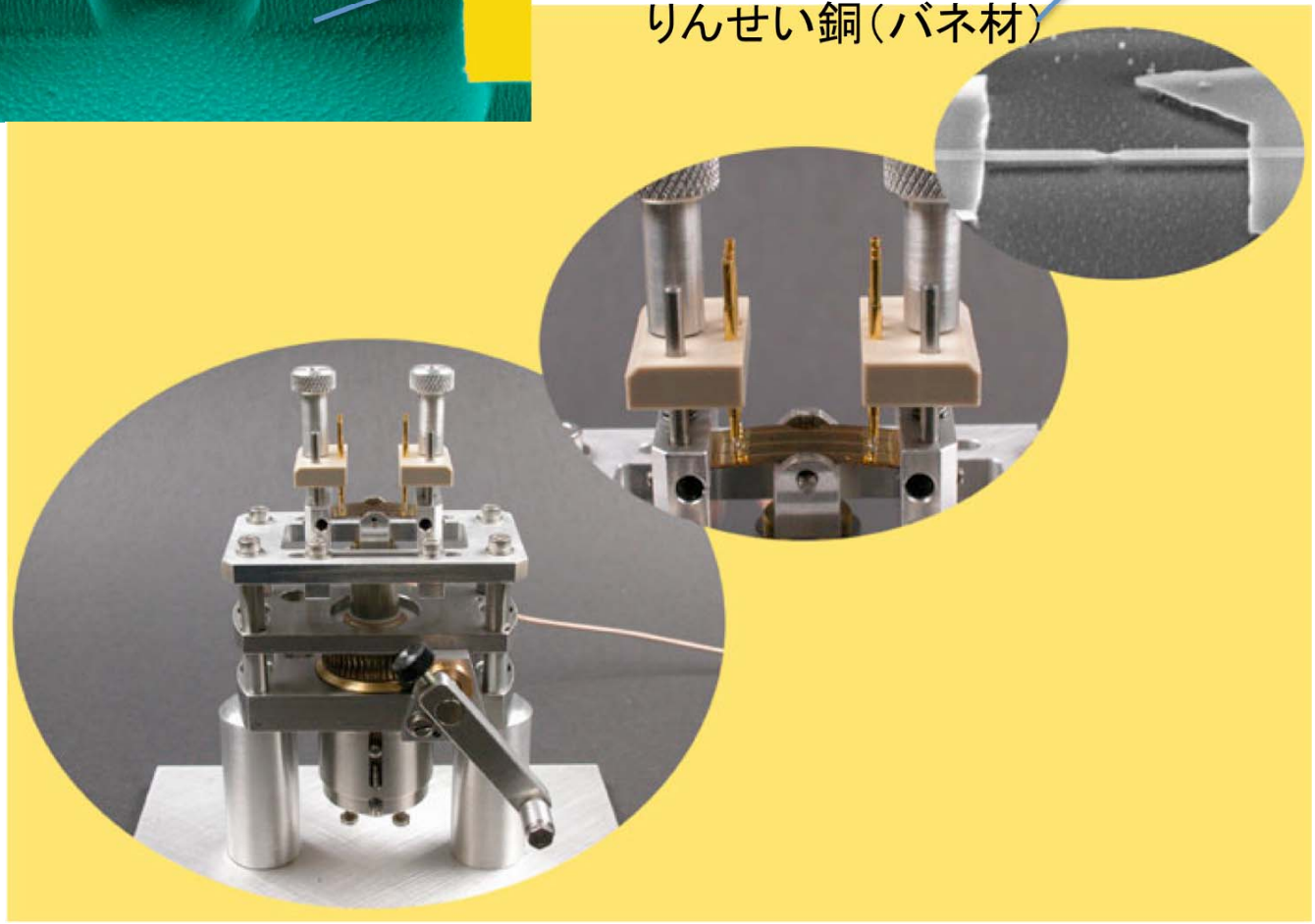

MCBJができそうな市販品

dsm
Mission Critical Motion Control™

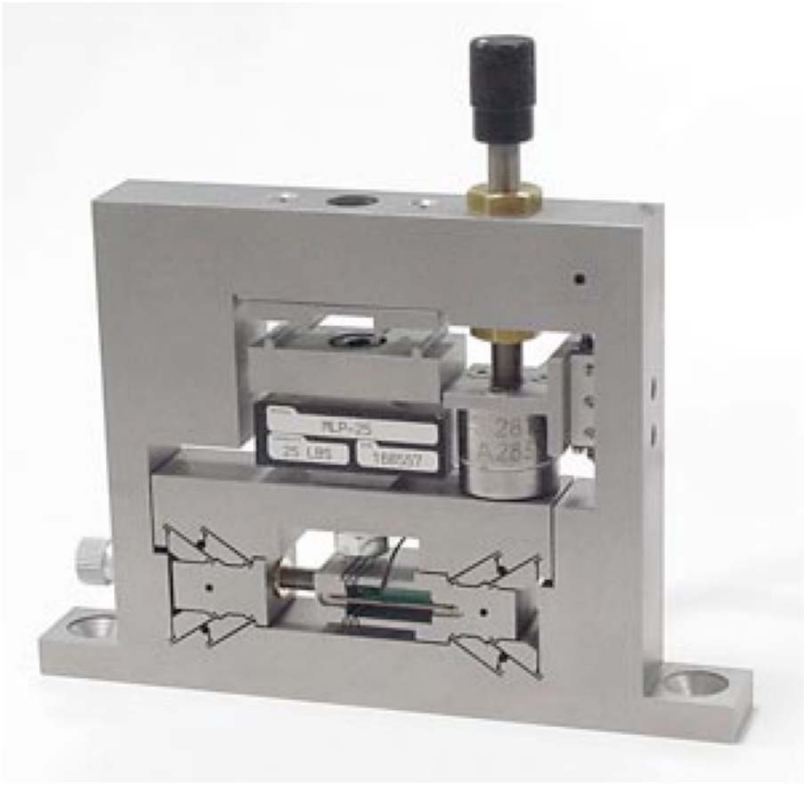

市販のベンディングマシン

分子エレクトロニクスを盛り上げて、盛り下げた論文

Retracted 1 November 2002; see last page

Science
AAAS

Field-Effect Modulation of the Conductance of Single Molecules

Jan Hendrik Schön, *et al.*

Science **294**, 2138 (2001);
DOI: 10.1126/science.1066171

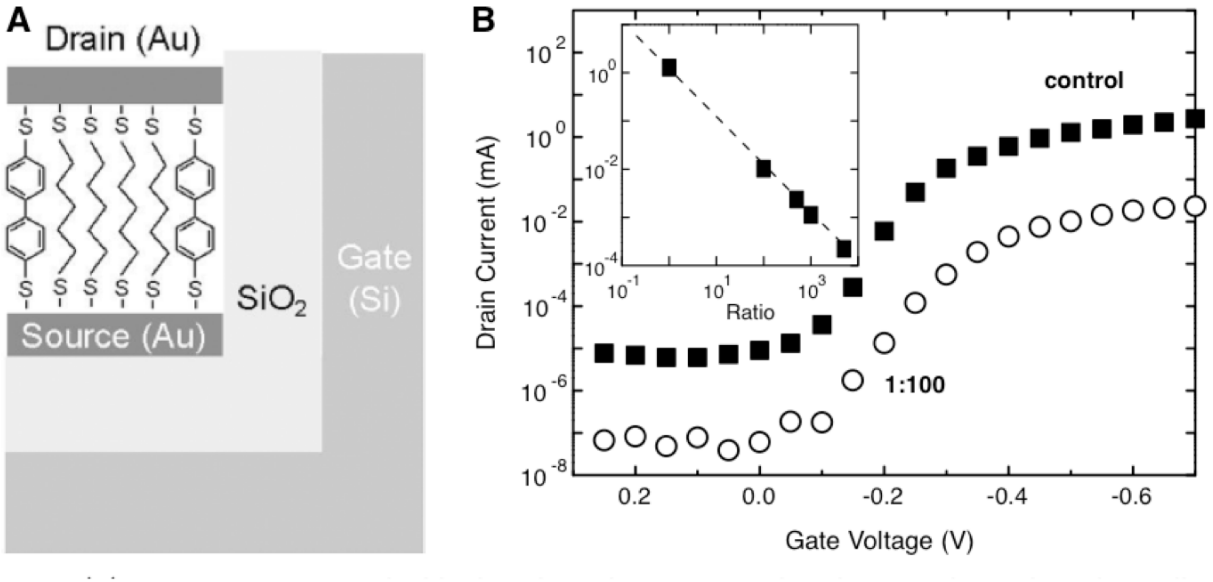

分子エレクトロニクスで最も良く出てくる論文だが…

Kondo resonance in a single-molecule transistor

Wenjie Liang*, Matthew P. Shores†, Marc Bockrath*, Jeffrey R. Long† & Hongkun Park*

** Department of Chemistry and Chemical Biology, Harvard University, 12 Oxford Street, Cambridge, Massachusetts 02138, USA*
† Department of Chemistry, University of California, Berkeley, California 94720, USA

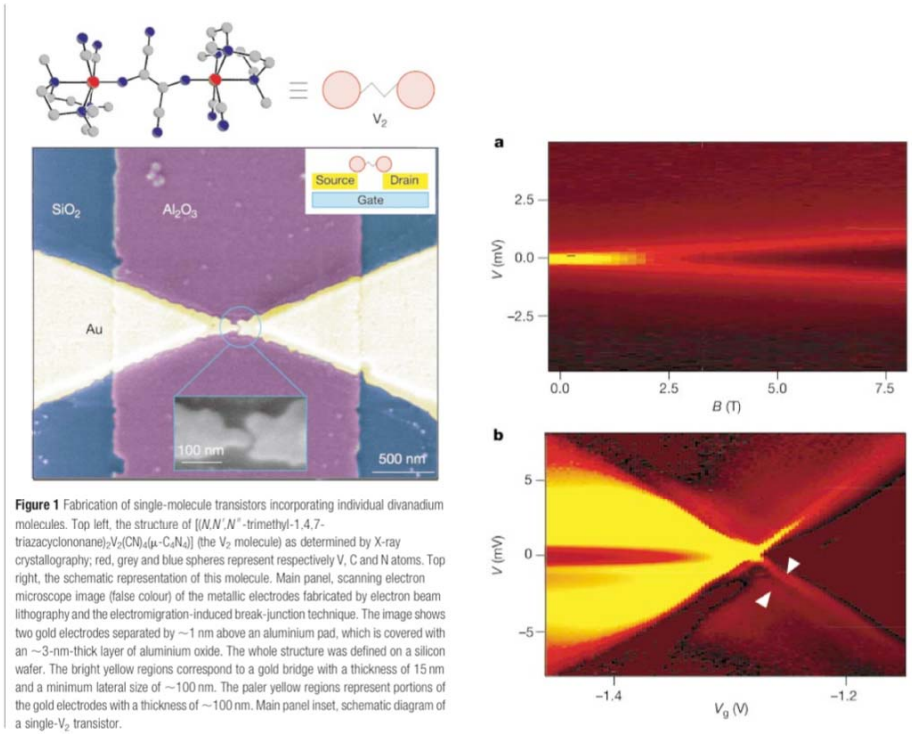

Figure 1 Fabrication of single-molecule transistors incorporating individual divanadium molecules. Top left, the structure of $[(N,N',N''\text{-trimethyl-1,4,7-triazacyclononane})_2V_2(CN)_4(\mu\text{-}C_4N_4)]$ (the V_2 molecule) as determined by X-ray crystallography; red, grey and blue spheres represent respectively V, C and N atoms. Top right, the schematic representation of this molecule. Main panel, scanning electron microscope image (false colour) of the metallic electrodes fabricated by electron beam lithography and the electromigration-induced break-junction technique. The image shows two gold electrodes separated by ~1 nm above an aluminium pad, which is covered with an ~3-nm-thick layer of aluminium oxide. The whole structure was defined on a silicon wafer. The bright yellow regions correspond to a gold bridge with a thickness of 15 nm and a minimum lateral size of ~100 nm. The paler yellow regions represent portions of the gold electrodes with a thickness of ~100 nm. Main panel inset, schematic diagram of a single-V_2 transistor.

Coulomb blockade and the Kondo effect in single-atom transistors

Jiwoong Park*†‡, Abhay N. Pasupathy*‡, Jonas I. Goldsmith§, Connie Chang*, Yuval Yaish*, Jason R. Petta*, Marie Rinkoski*, James P. Sethna*, Héctor D. Abruña§, Paul L. McEuen* & Daniel C. Ralph*

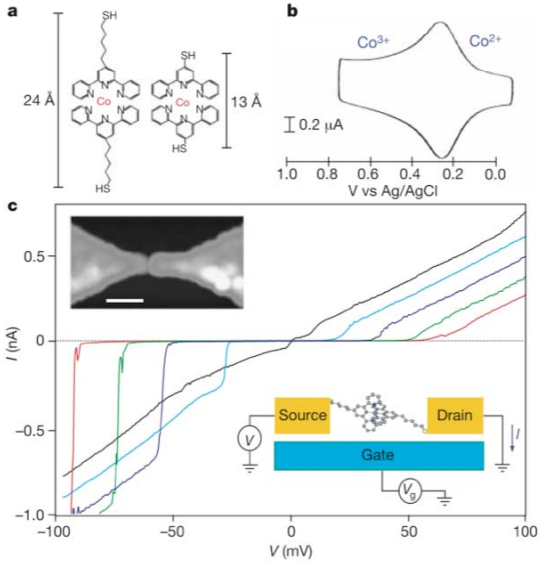

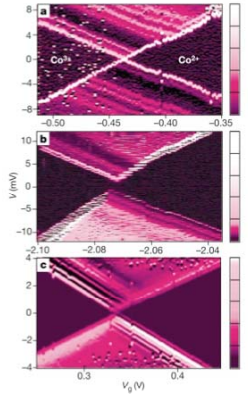

NATURE | VOL 417 | 13 JUNE 2002 | www.nature.com/nature

エレクトロマイグレーションはあやしい。

NANO LETTERS

2005
Vol. 5, No. 9
1685−1688

Kondo Effect in Electromigrated Gold Break Junctions

A. A. Houck,[†,‡] J. Labaziewicz,[†] E. K. Chan,[†] J. A. Folk,[*,†] and I. L. Chuang[†]

Center for Bits and Atoms and Department of Physics, Massachusetts Institute of Technology, Cambridge, Massachusetts 02139, and Department of Physics, Harvard University, Cambridge, Massachusetts 02138

Received April 29, 2005; Revised Manuscript Received July 12, 2005

We present gate-dependent transport measurements of Kondo impurities in bare gold break junctions, generated electromigration process that is actively controlled. Thirty percent of measured devices show zero-bias conduct dependence suggests Kondo temperatures ~7 K. The peak splitting in magnetic field is consistent with theoretic though in many devices the splitting is offset from $2g\mu_B B$ by a fixed energy. The Kondo resonances observed he scale metallic grains formed during electromigration.

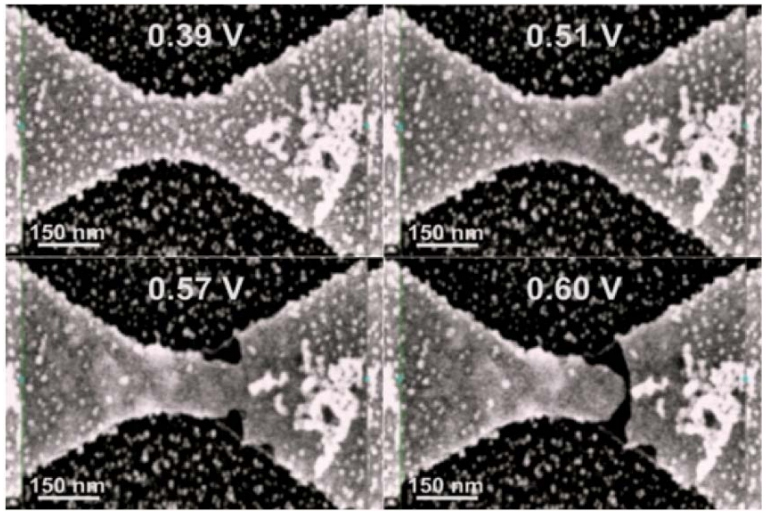

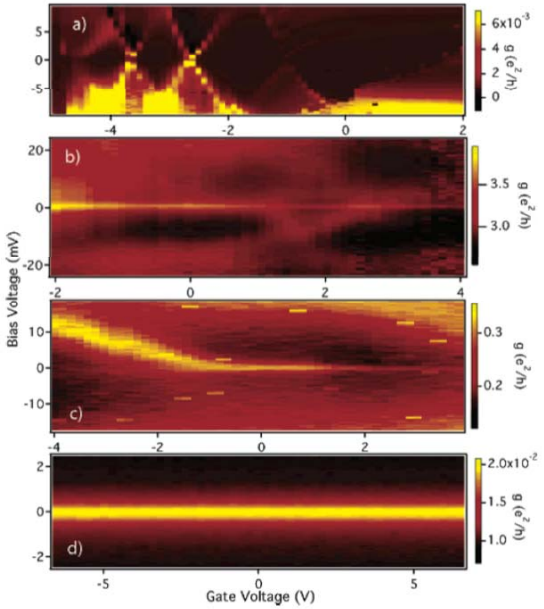

Figure 2. Differential conductance maps for four devices at 250 mK. (a) Coulomb blockade. (b) Superposition of a broad Coulomb blockade diamond (centered around gate voltage 1.8 V) and the Kondo effect. (c) Transition from Kondo resonance to Coulomb diamond. The absence of conductance features at negative bias may be due to an asymmetric lead coupling. (d) Gate-independent Kondo effect. (e) Numerical derivative of dc measurements; others measured with 50 μV ac bias at 47 Hz.

Figures from website

最近はよりよいとされるEMが開発された

単一分子計測の難しさ

「単分子のような」挙動を与える構造

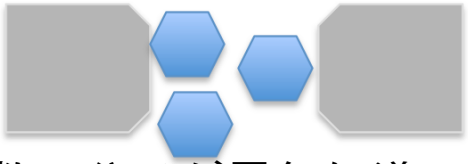

複数の分子が電気伝導に寄与

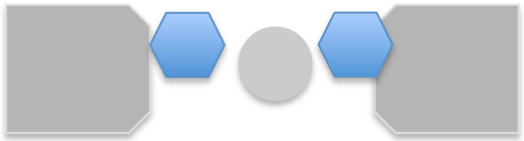

電極作成時に生じた「金属カス」が
電気伝導に寄与

分子の存在を示すには？

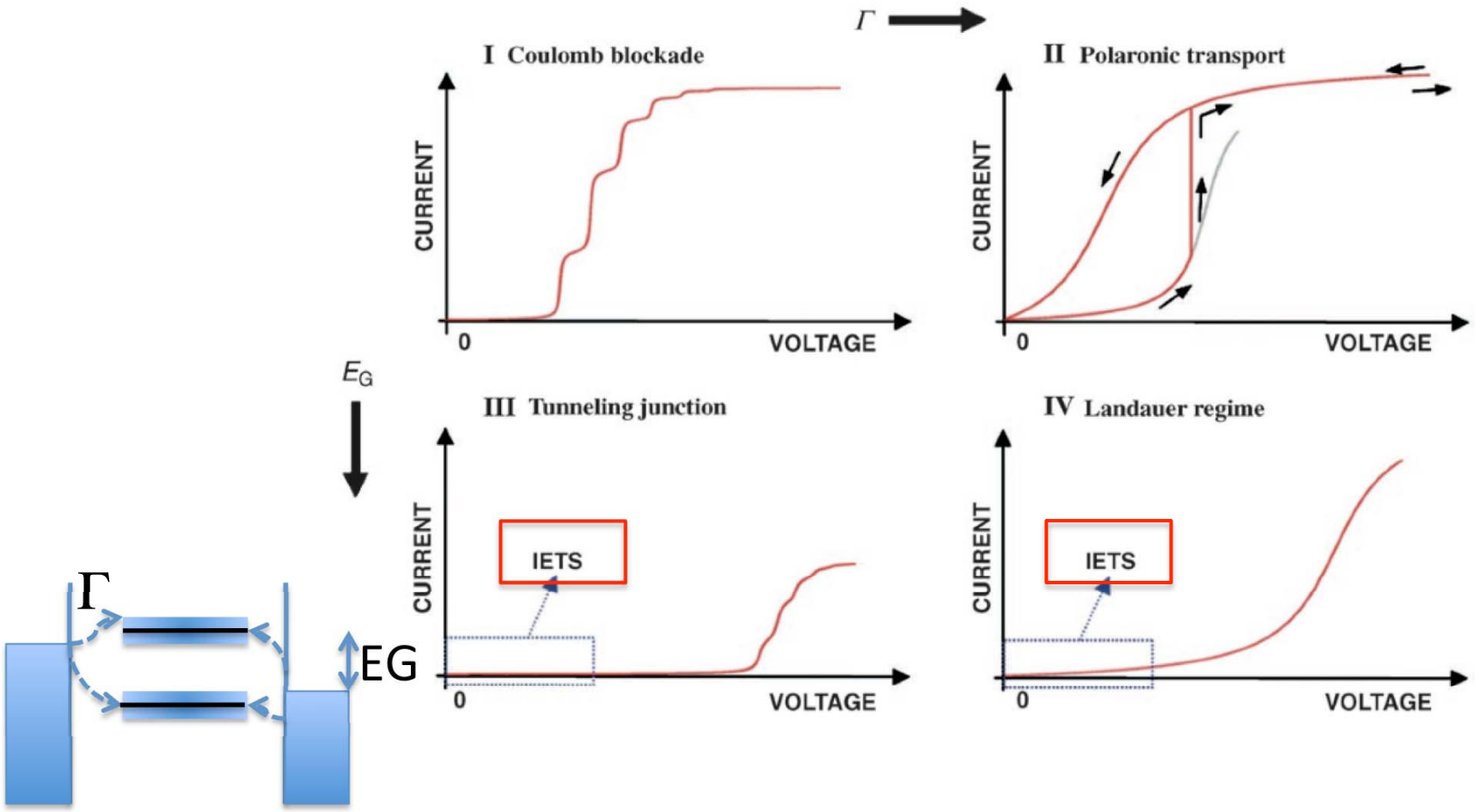

Troisi and Ratner, small, 2, 172, 2006.

Inelastic tunneling spectroscopyによる分子種の同定

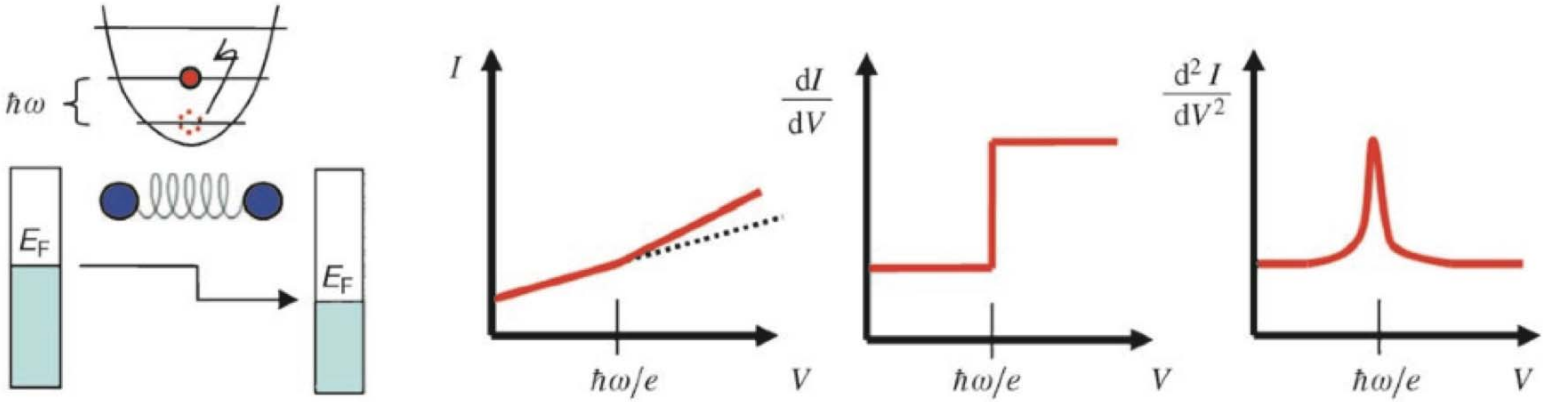

Figure 1. Illustration of the principle of inelastic electron tunneling spectroscopy (IETS): If the difference in chemical potential between the two electrodes is larger than the vibrational energy of one molecular mode, the electron can cross the junction losing one quantum of vibrational energy. This additional inelastic channel causes a small increase in conductance at $V=\hbar\omega/e$, better evaluated as a peak in a plot of d^2I/dV^2 versus V.

分子計測のお手本

Nature, 419, 906, 2002.

Measurement of the conductance of a hydrogen molecule

R. H. M. Smit*, Y. Noat*†, C. Untiedt*, N. D. Lang‡, M. C. van Hemert§ & J. M. van Ruitenbeek*

* *Kamerlingh Onnes Laboratorium, Universiteit Leiden, PO Box 9504, 2300 RA Leiden, The Netherlands*
‡ *IBM Research Division, Thomas J. Watson Research Center, Yorktown Heights, New York 10598, USA*
§ *Leids Instituut voor Chemisch Onderzoek, Gorlaeus Laboratorium, Universiteit Leiden, PO Box 9502, 2300 RA Leiden, The Netherlands*

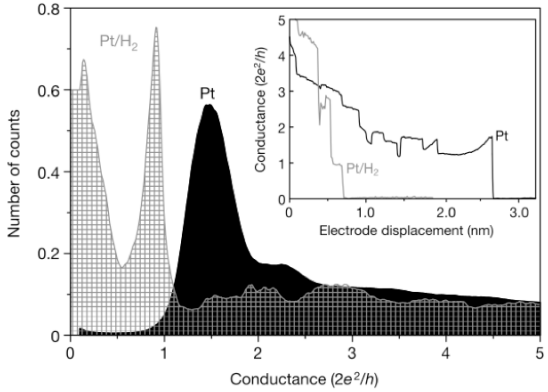

Figure 1 Conductance curves and histograms for clean Pt, and for Pt in a H_2 atmosphere. Inset, a conductance curve for clean Pt (black line) at 4.2 K recorded with a bias voltage of 10 mV, before admitting H_2 gas into the system. About 10,000 similar curves are used to build the conductance histogram shown in the main panel (black), which has been normalized by the area under the curve. After introducing H_2 gas, the conductance curves change qualitatively as illustrated by the grey curve in the inset, recorded at 100 mV. This is most clearly brought out by the conductance histogram (grey; recorded with 140 mV bias). Briefly, the mechanically controllable break-junction technique works as follows. Starting with a macroscopic metal wire, a notch is formed by incision with a knife. The samples are mounted inside a vacuum container and pumped to a pressure below 5×10^{-7} mbar. Next, the system is cooled to 4.2 K in order to attain a cryogenic vacuum. After cooling, the sample wire is broken at the notch by bending of the substrate onto which it has been fixed. The clean, freshly exposed fracture surfaces are then brought back into contact by slightly relaxing the bending. With the use of a piezoelectric element, the displacement of the two electrodes can be finely adjusted to form a stable contact of atomic size. A thick copper finger provides thermal contact to the sample inside the container.

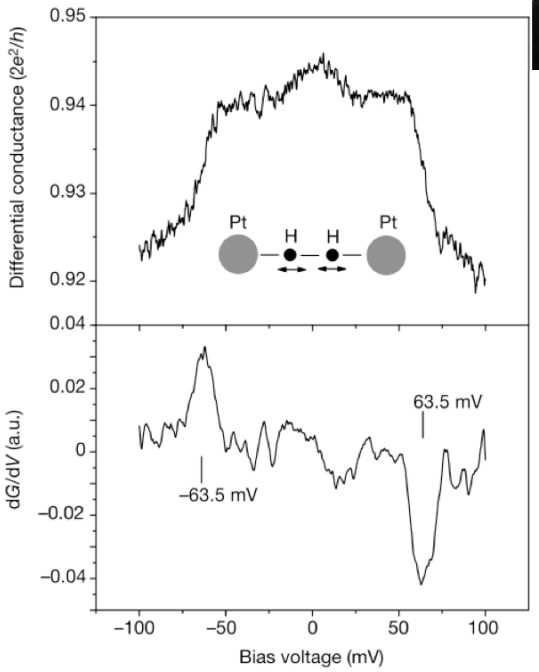

Figure 2 Differential conductance (top) and its derivative (bottom) for a Pt/H_2 contact taken at a conductance plateau close to $1G_0$. The differential conductance is recorded by a lock-in amplifier using a modulation amplitude between 0.88 and 1.5 mV_{rms} at 7 kHz and a time constant of 10 ms, and the derivative is numerically calculated. A full spectrum is recorded in 10 s.

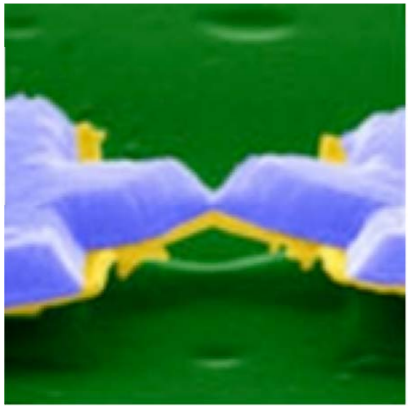

前ページより続く

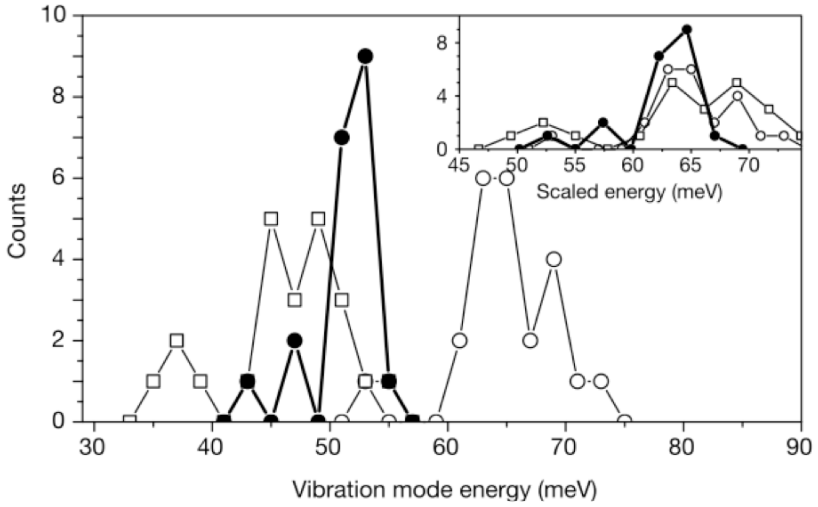

Figure 3 Vibration mode energies obtained from point contact spectra similar to that shown in Fig. 2. Open circles, Pt/H_2; open squares, Pt/D_2; filled circles, Pt/HD. The vertical scale shows the number of spectra with energies within a bin size of 2 meV. The inset shows the same data with the energy axis scaled by the factors expected for the isotope shifts of the hydrogen molecule, $\omega_{H_2}/\omega_{D_2} \propto \sqrt{m_{D_2}/m_{H_2}} = \sqrt{2} \approx 1.414$ (open squares), and $\omega_{H_2}/\omega_{HD} \propto \sqrt{m_{HD}/m_{H_2}} = \sqrt{3/2} \approx 1.225$ (filled circles).

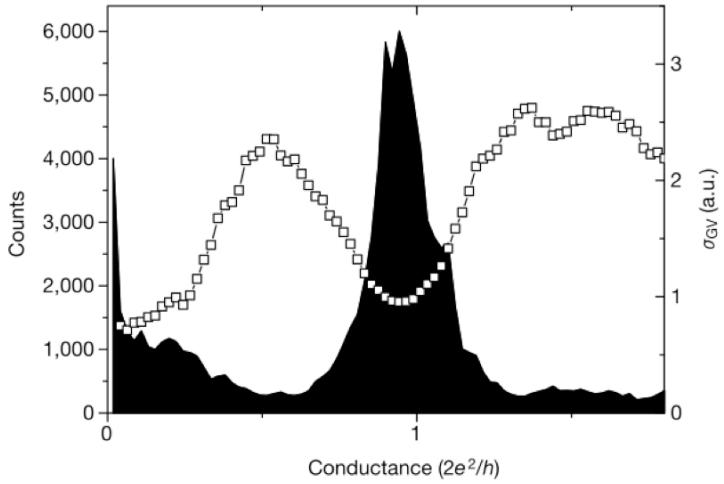

Figure 4 Conductance histogram (black, left axis) and r.m.s. amplitude of the conductance fluctuations σ_{GV} (open squares, right axis) for a Pt/H_2 sample. These data were obtained using 2,000 cycles of contact breaking. The conductance and its derivative were measured with two parallel lock-in amplifiers, detecting the frequencies f and $2f$, with 140 mV bias voltage and 20 mV modulation amplitude. The derivative signal is used to calculate the average of the conductance fluctuations, σ_{GV}, and each of the points is obtained from the data belonging to one bin of the histogram.

現在の標準的な測定方法

Science
AAAS

Measurement of Single-Molecule Resistance by Repeated Formation of Molecular Junctions

Bingqian Xu, *et al.*

Science **301**, 1221 (2003);
DOI: 10.1126/science.1087481

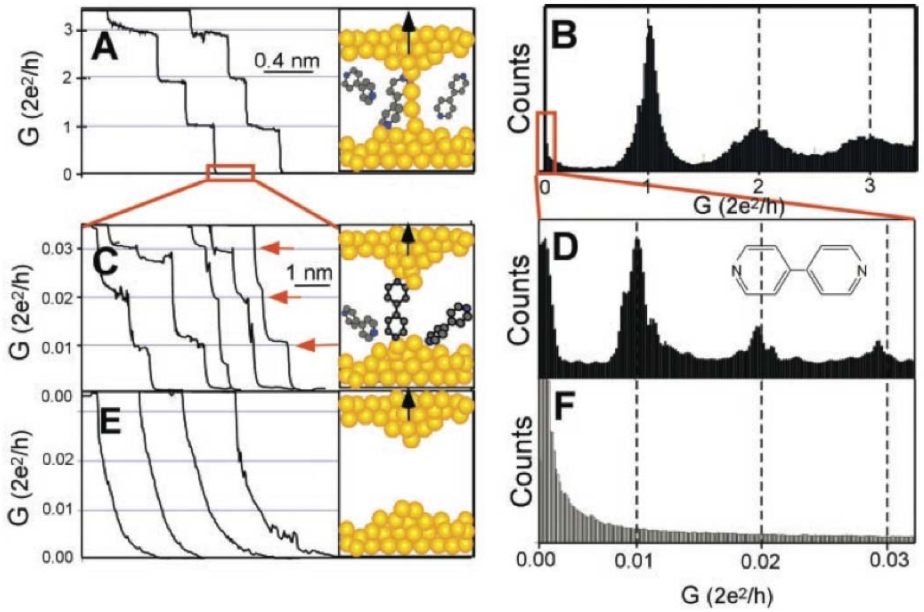

Fig. 1. (**A**) Conductance of a gold contact formed between a gold STM tip and a gold substrate decreases in quantum steps near multiples of G_0 ($= 2e^2/h$) as the tip is pulled away from the substrate. (**B**) A corresponding conductance histogram constructed from 1000 conductance curves as shown in (A) shows well-defined peaks near 1 G_0, 2 G_0, and 3 G_0 due to conductance quantization. (**C**) When the contact shown in (A) is completely broken, corresponding to the collapse of the last quantum step, a new series of conductance steps appears if molecules such as 4,4′ bipyridine are present in the solution. These steps are due to the formation of the stable molecular junction between the tip and the substrate electrodes. (**D**) A conductance histogram obtained from 1000 measurements as shown in (C) shows peaks near 1 ×, 2 ×, and 3 × 0.01 G_0 that are ascribed to one, two, and three molecules, respectively. (**E** and **F**) In the absence of molecules, no such steps or peaks are observed within the same conductance range.

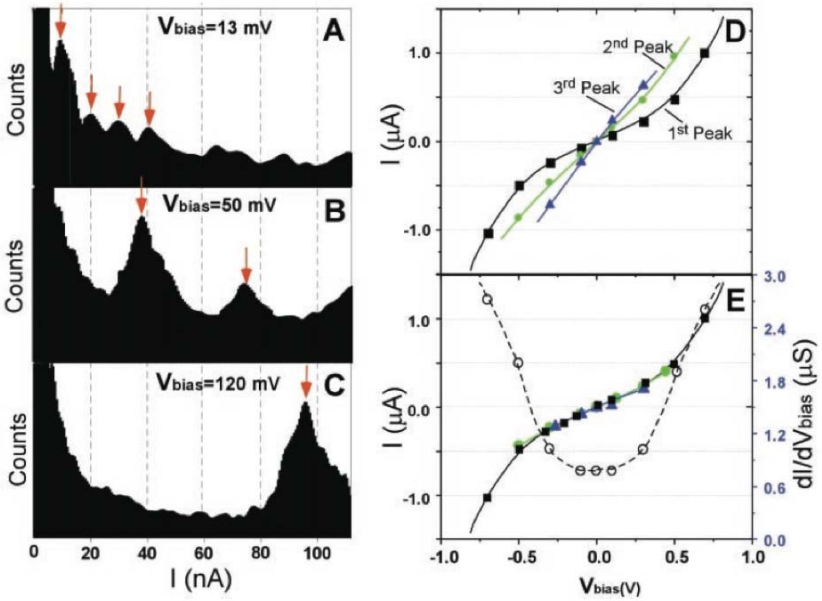

Fig. 2. (**A** to **C**) Current histograms of 4,4′ bipyridine constructed from 1000 measurements at different bias voltages (V_{bias}). Peak currents increase with the bias voltage and are used to obtain characteristic *I-V* curves. (**D**) *I-V* curves from the first three peaks. (**E**) When the second peak is divided by 2 and the third peak by 3, all the three curves collapse into a single curve. The dashed line shows the differential conductance (dI/dV).

分子の電気伝導度の測り方

Break Junction 法

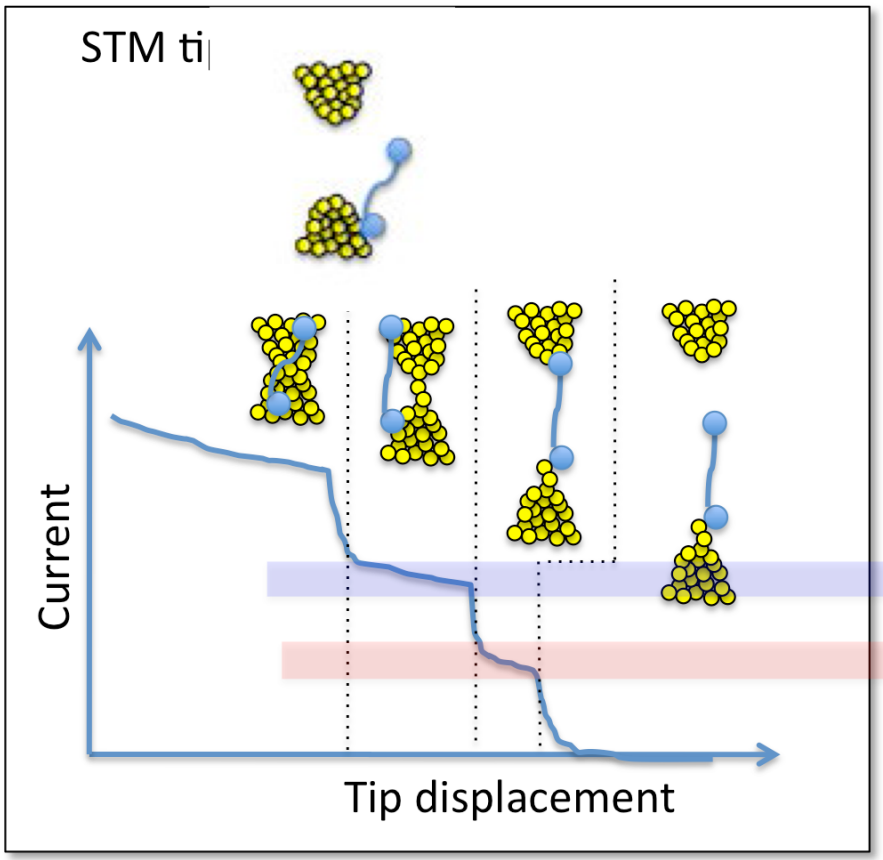

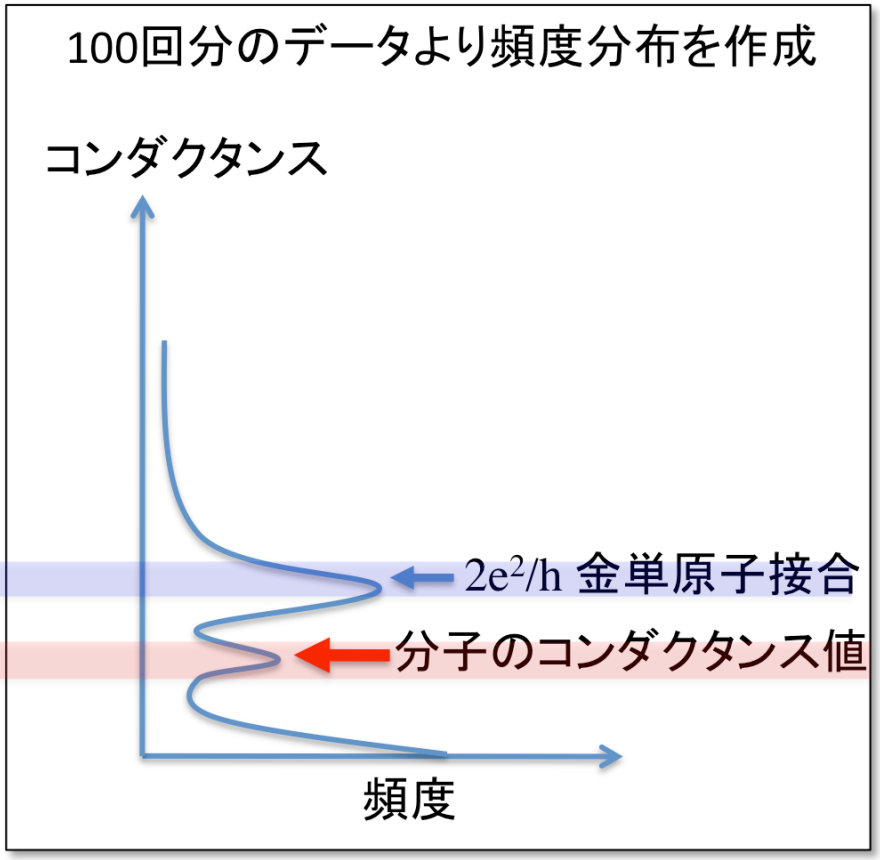

もっとも頻度の高いコンダクタンス値を分子のコンダクタンスと解釈する。

「単分子を測った」と言うための条件

- 数多くのデーターの頻度分析をする
  →信頼性
- 破断過程で不連続な変化を示している
  →任意のトンネル接合ではない
- ある基数の整数倍のコンダクタンスが現れることを示す
  →分子の数
- 比較対照実験をする
  →分子の存在
- 非弾性信号から振動スペクトルを評価する
  →分子の存在
- ノイズ分析からコンダクタンスチャネルを評価する
  → 分子を介した伝導

単一分子計測の難しさ

「単分子のような」挙動を与える構造

複数の分子が電気伝導に寄与

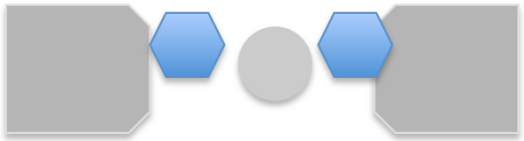

電極作成時に生じた「金属カス」が電気伝導に寄与

ミクロな構造ゆらぎにより電気伝導度が一義的に決まらない。

コンタクトの構造　　結合の角度

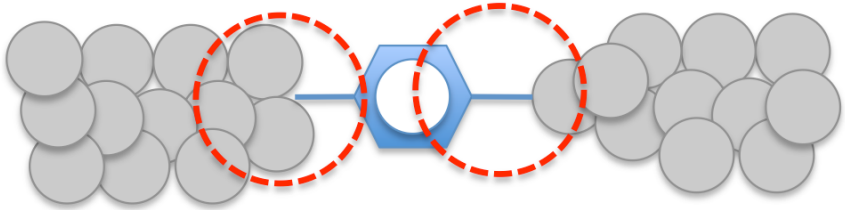

はじめの研究対象

コンタクトの種類と構造

STM-BJ

Effect of Anchoring Groups on Single-Molecule Conductance: Comparative Study of Thiol-, Amine-, and Carboxylic-Acid-Terminated Molecules

Fang Chen, Xiulan Li, Joshua Hihath, Zhifeng Huang, and Nongjian Tao*

Department of Electrical Engineering & Center for Solid State Electronics Research, Arizona State University, Tempe, Arizona 85287

Received August 11, 2006; E-mail: nongjian.tao@asu.edu

JACS, 128, 15874, 2006.

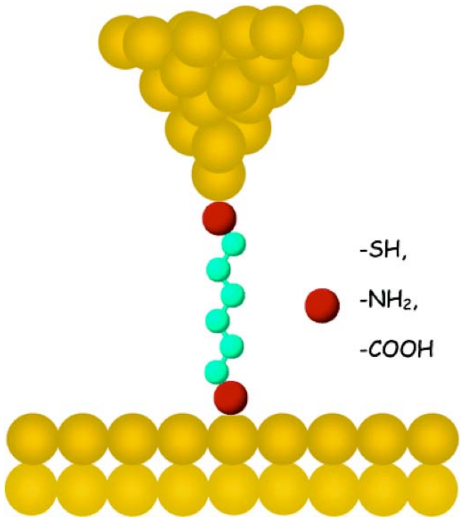

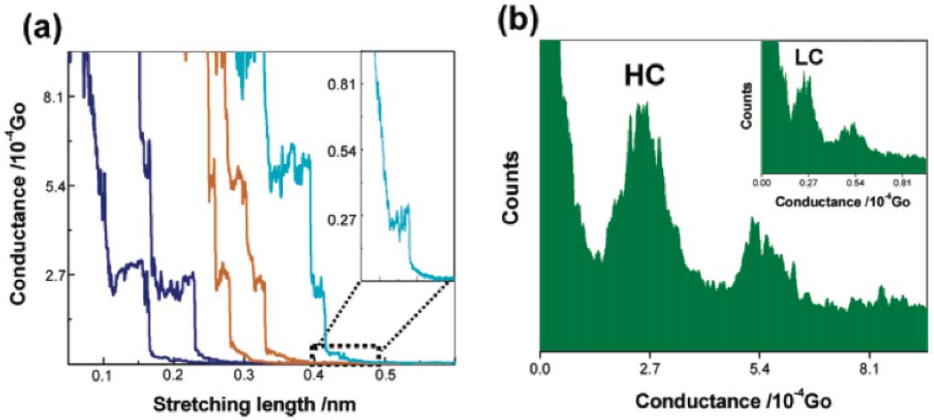

Hi and Lo conductance states

Contact conductance: Au-S > Au-NH2 > Au-COOH

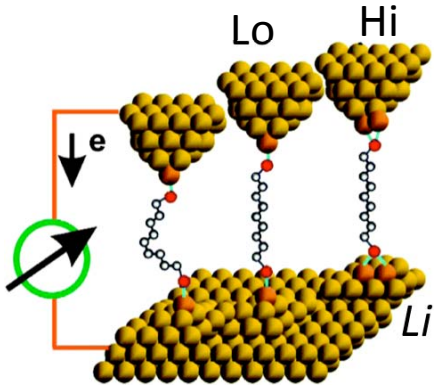

(人によってはさらに小さい値
の三種類があると言っている）

Li et al, J. Am. Chem. Soc., ***2008, 130 (1), pp 318–326***

分子（π結合）のねじれ

STM-BJ

Dependence of single-molecule junction conductance on molecular conformation

Nature, 442, 904, 2006.

Latha Venkataraman[1,4], Jennifer E. Klare[2,4], Colin Nuckolls[2,4], Mark S. Hybertsen[3,4] & Michael L. Steigerwald[2]

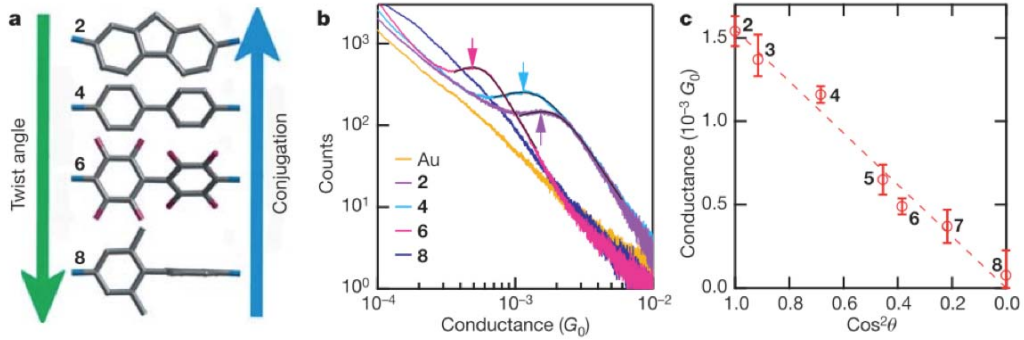

Table 1 | Molecular structure and measured properties

Molecule number	Structure	Conductance (G_0) Measured	Conductance (G_0) Calculated	Peak width*	Twist angle (°)
1	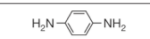	6.4×10^{-3}	6.4×10^{-3}	0.4	–
2	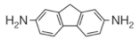	1.54×10^{-3}	2.1×10^{-3}	0.8	0
3	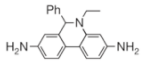	1.37×10^{-3}	2.2×10^{-3}	0.8	17
4	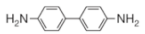	1.16×10^{-3}	1.6×10^{-3}	0.9	34
5	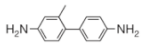	6.5×10^{-4}	1.2×10^{-3}	1.3	48
6	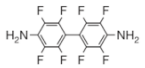	4.9×10^{-4}	7.1×10^{-4}	0.6	52
7	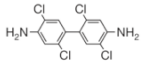	3.7×10^{-4}	5.8×10^{-4}	0.9	62
8		7.6×10^{-5}†	6.4×10^{-5}	NA†	88
9	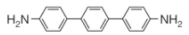	1.8×10^{-4}‡	3.5×10^{-4}	2.1	–

Table shows molecule structure, measured conductances, calculated relative conductances, relative widths of the histogram peaks (see Supplementary Information for details) and the calculated twist angle, θ.
*Half-width at half-maximum of the lorentzian fit, normalized to the peak value.
†The histogram peak was determined after subtracting the Au histogram from the data, as the raw data could not be fitted with a lorentzian so a width could not be determined.
‡Determined from actual maximum of the raw data.

ねじれ角依存性

コンタクトの角度

STM-BJ（ちょっとちがう）

Precision control of single-molecule electrical junctions

WOLFGANG HAISS[1]*, CHANGSHENG WANG[2], IAIN GRACE[3], ANDREI S. BATSANOV[2], DAVID J. SCHIFFRIN[1], SIMON J. HIGGINS[1], MARTIN R. BRYCE[2], COLIN J. LAMBERT[3] AND RICHARD J. NICHOLS[1]

[1]Centre for Nanoscale Science and Department of Chemistry, University of Liverpool, L69 7ZD, UK
[2]Department of Chemistry and Centre for Molecular and Nanoscale Electronics, University of Durham, Durham DH1 3LE, UK
[3]Department of Physics, Lancaster University, Lancaster LA1 4YB, UK
*e-mail: w.h.haiss@liv.ac.uk

結合角依存性

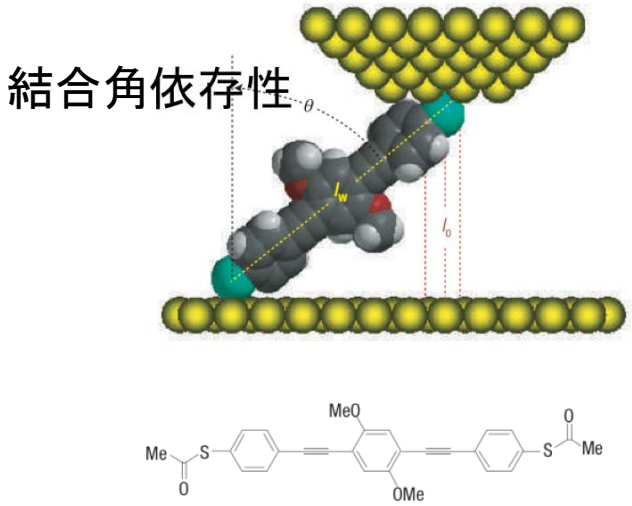

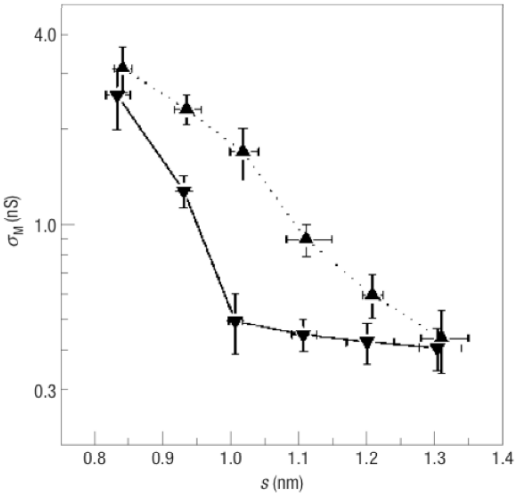

Figure 3 Single-molecule conductance. Nonanedithiol measured at 75 °C (up triangles) and 28 °C (down triangles) in dependence on s at $U_{tip} = +0.6$ V. Error bars represent the standard deviation of group 1 events.

Nature Materials, 5, 995, 2006.

力学測定と電流による局所加熱問題

STM(AFM)-BJ

Measurement of Current-Induced Local Heating in a Single Molecule Junction

Zhifeng Huang,† Bingqian Xu,† Yuchang Chen,§ Massimiliano Di Ventra,*,‡ and Nongjian Tao*,†

Nano Lett. 6, 1240, 2006.

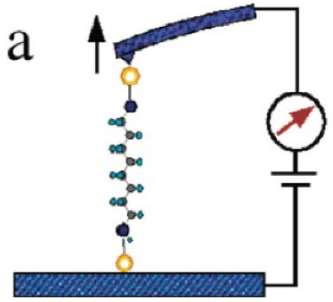

AFMで力測定をしながら計測

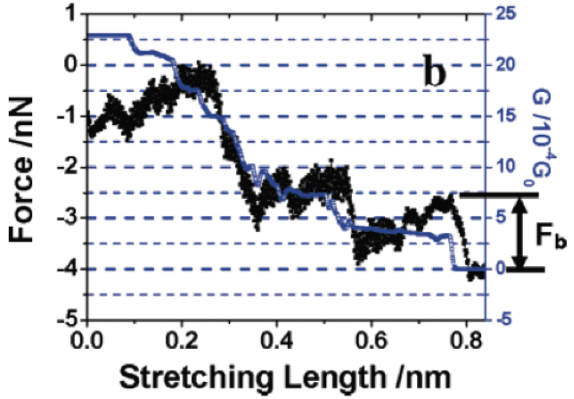

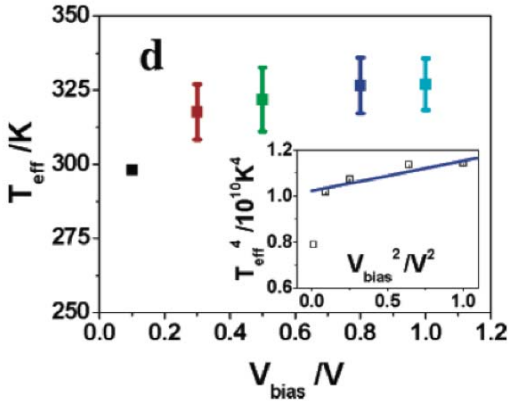

置換基による分子準位シフトの効果

STM-BJ

Electronics and Chemistry: Varying Single-Molecule Junction Conductance Using Chemical Substituents

Latha Venkataraman,*,†,|| Young S. Park,‡,|| Adam C. Whalley,‡,|| Colin Nuckolls,‡,||
Mark S. Hybertsen,§,||,⊥ and Michael L. Steigerwald‡

Nano Lett., 7, 502, 2007.

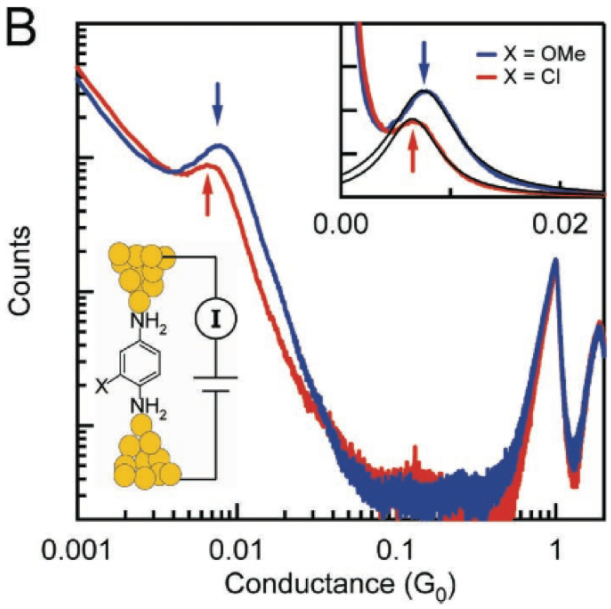

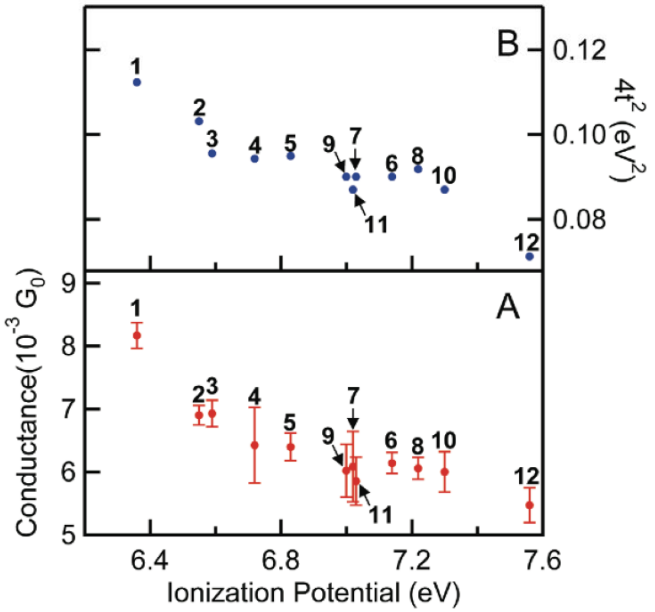

Figure 2. (A) Measured conductance values against the calculated ionization potential for the series of 12 molecules tested. The number of traces measured ranged from 12 000 to 30 000 for different molecules. For each molecule, histograms of 1000 consecutive traces were computed and a Lorentzian was fit to the molecular peak. The mean and standard deviation of the peak positions determined the molecule conductance and the error bar (also listed in Table 1). (B) Square of the calculated tunnel coupling ($4 \times t^2$) against the calculated ionization potential.

溶媒和効果

Single-Molecule Solvation-Shell Sensing

STM-BJ

E. Leary,[1] H. Höbenreich,[1] S. J. Higgins,[1] H. van Zalinge,[1] W. Haiss,[1] R. J. Nichols,[1] C. M. Finch,[2] I. Grace,[2] C. J. Lambert,[2] R. McGrath,[3] and J. Smerdon[3]

PRL, 102, 086801, 2009.

A

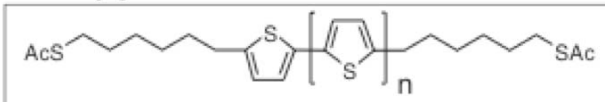

Molecule	Length (S...S, nm)
1. n = 0	1.99
2. n = 1	2.38
3. n = 2	2.72
4. n = 4	3.47

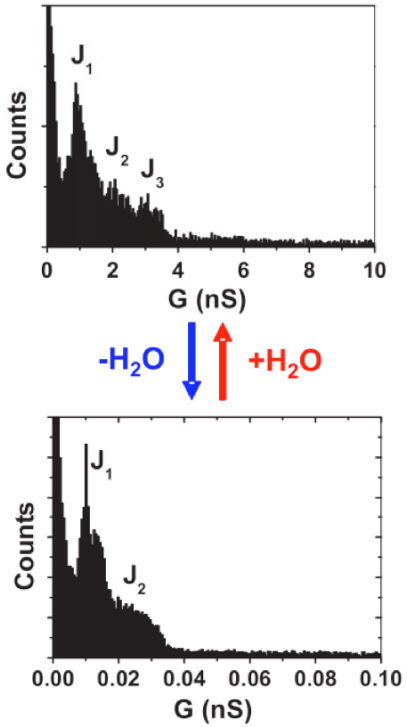

FIG. 2 (color online). Histogram of the characteristic current plateaus [$I(w)$] observed for molecule 3 measured under (lower) dry argon, $U_{tip} = +1$ V, set point current = 7 nA (upper) after subsequent readmission of ambient (wet) air to the STM chamber, same conditions.

水が配位するとコンダクタンス10倍

STM-BJ（統計的解析）からの情報

・コンタクトの配座によって桁違いのコンダクタンスを示す。
・コンタクトの角度によってコンダクタンスが変わる。
・分子のねじれ、折れ曲がりによってコンダクタンスが桁違いに変わる。

分子の機能を議論するときには、上記の状況がどのように影響したかを議論しなければならない。

STMで分子接合を（ひかくてき）安定に計測した例

安定な分子接合で直接測定した例： STMによる電気化学ゲート効果

STM

Electromechanical and Conductance Switching Properties of Single Oligothiophene Molecules

Bingqian Q. Xu,† Xiulan L. Li,† Xiaoyin Y. Xiao,† Hiroshi Sakaguchi,‡ and Nongjian J. Tao*,†

Department of Electrical Engineering & The Center for Solid State Electronics Research, Arizona State University, Tempe, Arizona 85287, and Research Institute of Electronics, Shizuoka University, Hamamatsu 432-8011, Japan

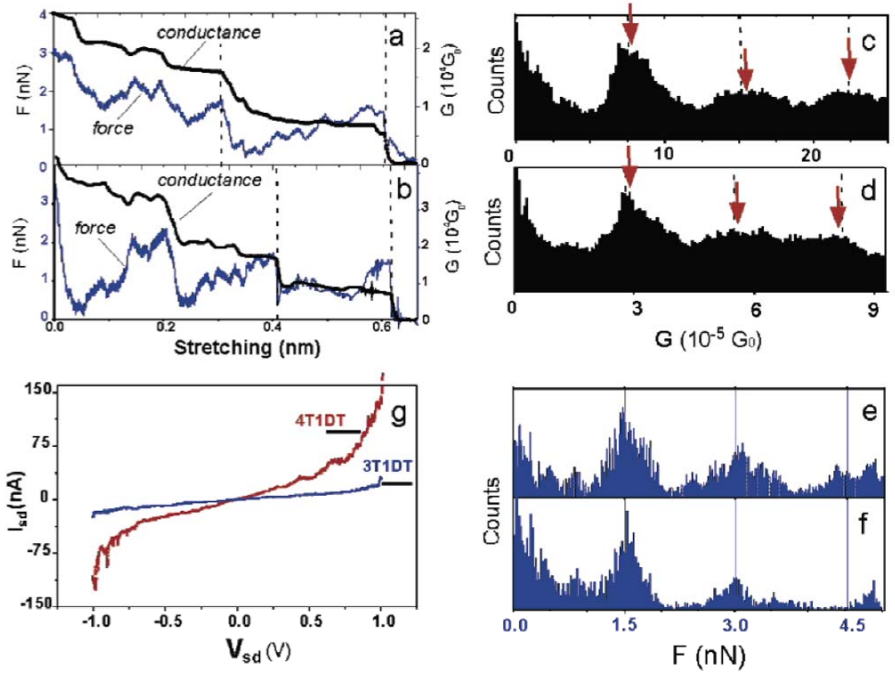

Figure 2. (a−b) Simultaneously measured conductance and force curves during individual stretching processes (stretching rate 40 nm/sec.) for 4T1DT in toluene solution. (c−d) Conductance histograms of 4T1DT (c) and 3T1DT (d) constructed using ~500 such curves as shown in a and b. (e−f) Breakdown force histograms of 4T1DT (c) and 3T1DT (d) constructed using ~500 such curves as shown in a and b. (g) *I*−*V* characteristic curves of 3T1DT and 4T1DT.

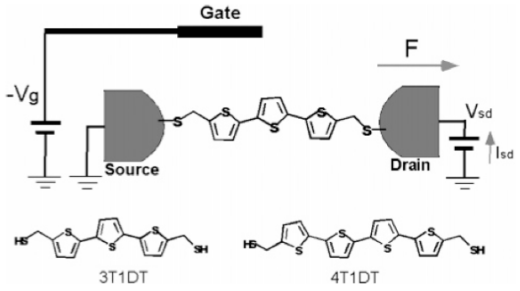

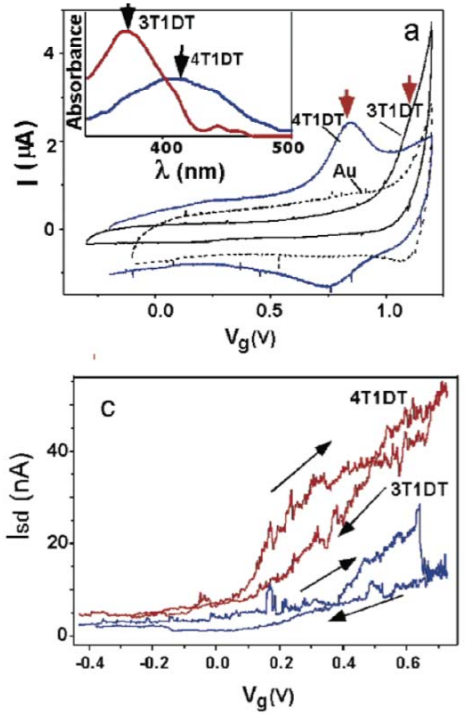

Figure 3. (a) Cyclic voltammograms of 3T1DT (black line) and 4T1DT (blue line) adsorbed on a gold electrode in 0.1 M $HClO_4$. The potential sweep rate is 0.2 V/sec. The arrows point to the reduction and reoxidation peaks of the two redox processes. For comparison, the voltammogram of a bare gold electrode is also shown (dashed line). Inset of (a) UV−vis spectroscopy of 3T1DT and 4T1DT molecules. (b) Conductance histograms of the 4T1DT molecule conductance in 0.1 M $NaClO_4$ at different gate voltages. (c) Source−drain current vs gate voltage for single 3T1DT and 4T1DT molecules obtained by recording the source−drain current while sweeping the gate voltage in 0.1 M $NaClO_4$.

熱電効果

STM

Thermoelectricity in Molecular Junctions

Pramod Reddy,[1]* Sung-Yeon Jang,[2,3]*† Rachel A. Segalman,[1,2,3]‡ Arun Majumdar[1,3,4]‡

Science, 315, 1568, 2007.

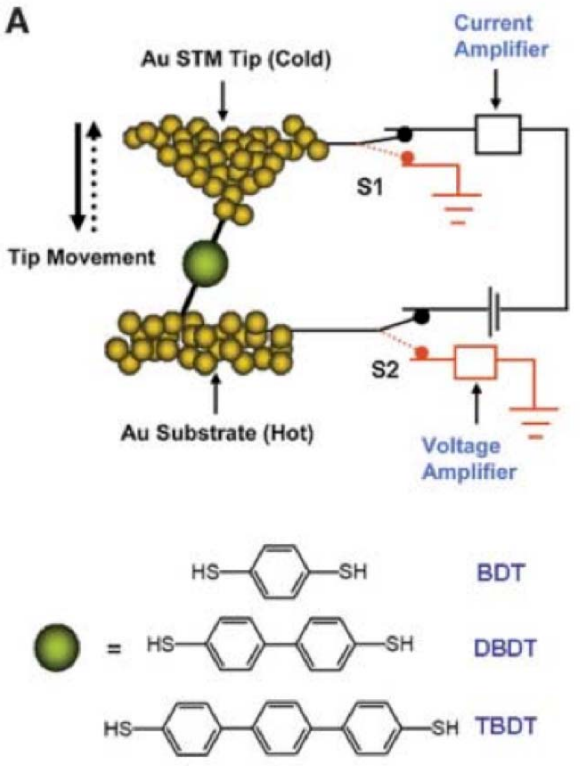

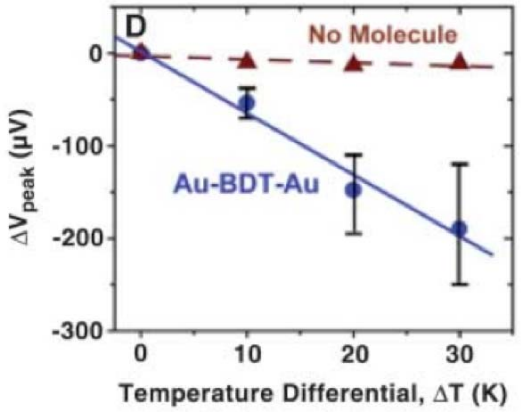

熱起電力

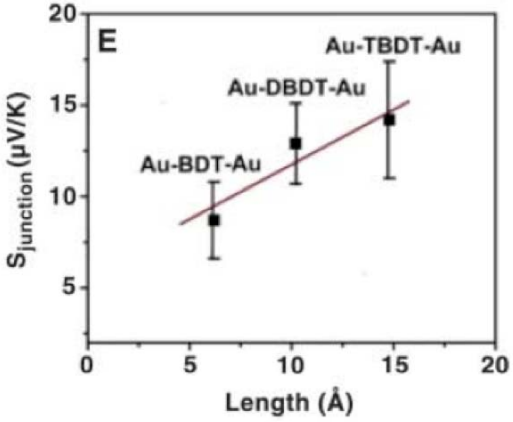

ゼーベック係数

整流特性

STM

Rectification and stability of a single molecular diode with controlled orientation

Ismael Díez-Pérez[1], Joshua Hihath[1], Youngu Lee[2†], Luping Yu[2*], Lyudmyla Adamska[3], Mortko A. Kozhushner[4], Ivan I. Oleynik[3] and Nongjian Tao[1*]

Nature Chemistry, 1, 635, 2009.

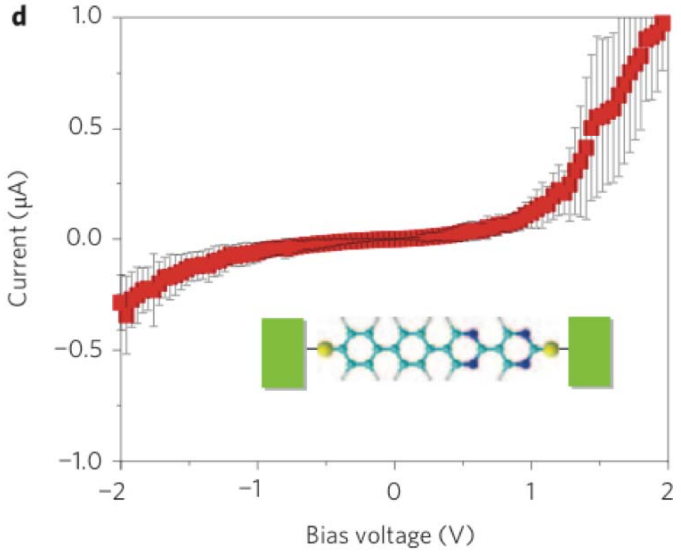

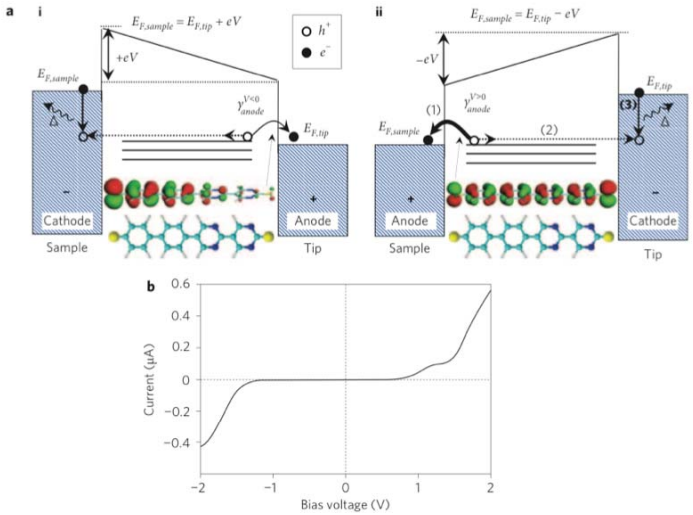

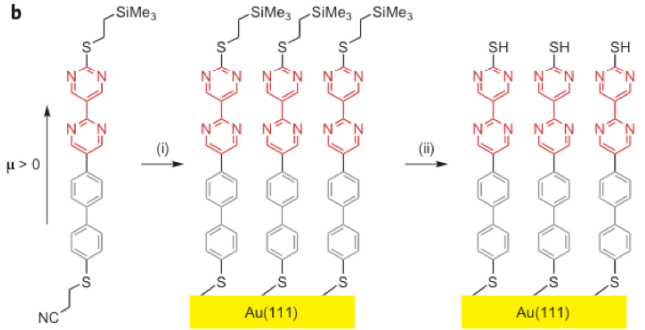

保護基を利用して分子配向を揃えた

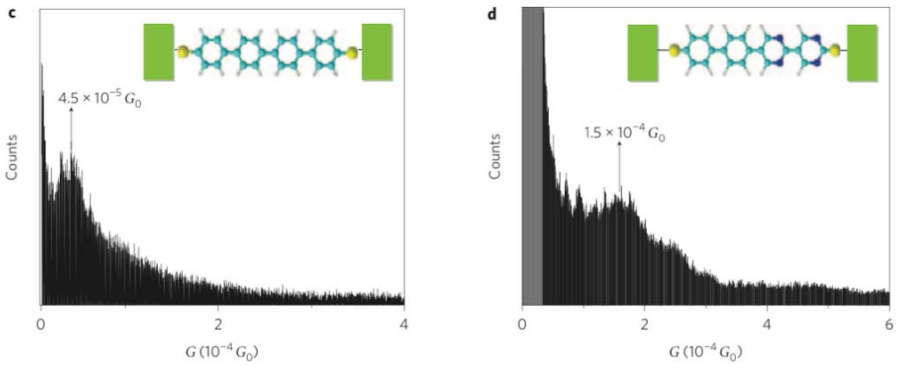

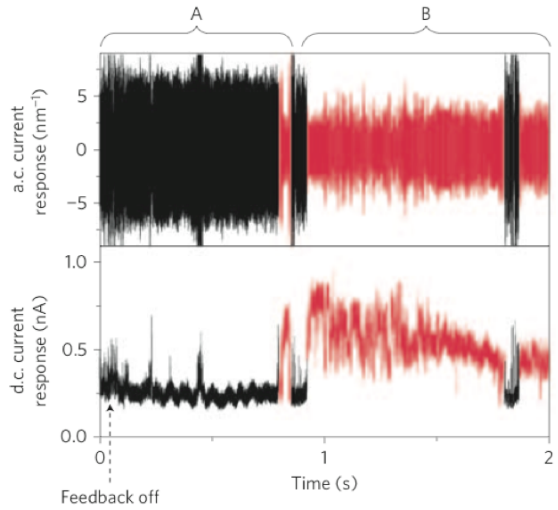

Figure 3 | Components of the current traces during a single dipyrimidinyl–diphenyl bridge formation. Regions A (black) and B (red) correspond to tunnelling by means of space and conduction, respectively, through the single-molecule junction. The dashed arrow indicates when the feedback was turned off. The initial setpoint current was 0.25 nA and the bias was 50 mV. The amplitude and frequency of the a.c. modulation were 0.06 nm and 2 kHz, respectively. The a.c.-response (nm^{-1}) is a normalized value as defined in the text.

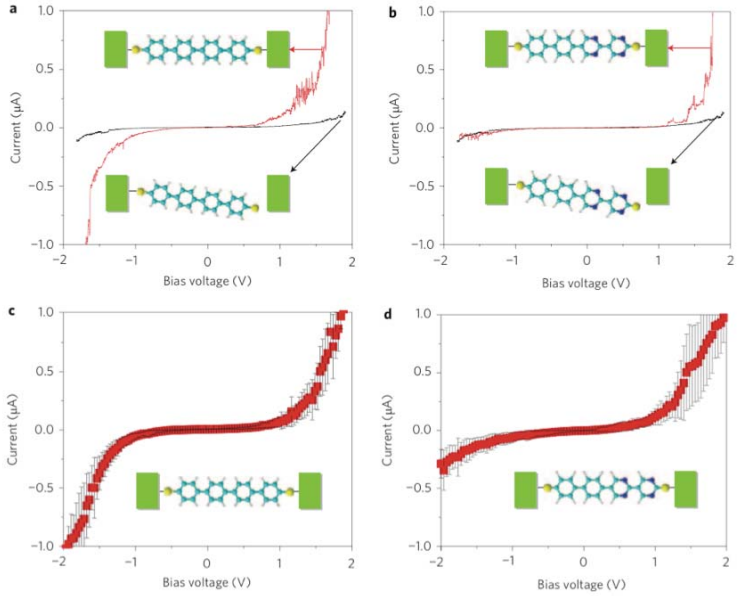

Figure 4 | Current-voltage (*I–V*) curves for the symmetric and non-symmetric molecules. a,b, The *I–V* curves were recorded in both regions A (gap junction, black) and B (single-molecule junction, red) of Fig. 3 for the symmetric tetraphenyl (**a**) and the non-symmetric dipyrimidinyl-diphenyl (**b**) molecules. **c,d**, Average curves for the single-molecule junctions built from 30 (**c**) and 50 (**d**) individual *I–V* curves, with error bars that represent standard deviation.

長い分子をつり上げる

STM

Conductance of a Single Conjugated Polymer as a Continuous Function of Its Length

Leif Lafferentz,[1] Francisco Ample,[2] Hao Yu,[3] Stefan Hecht,[3] Christian Joachim,[2] Leonhard G

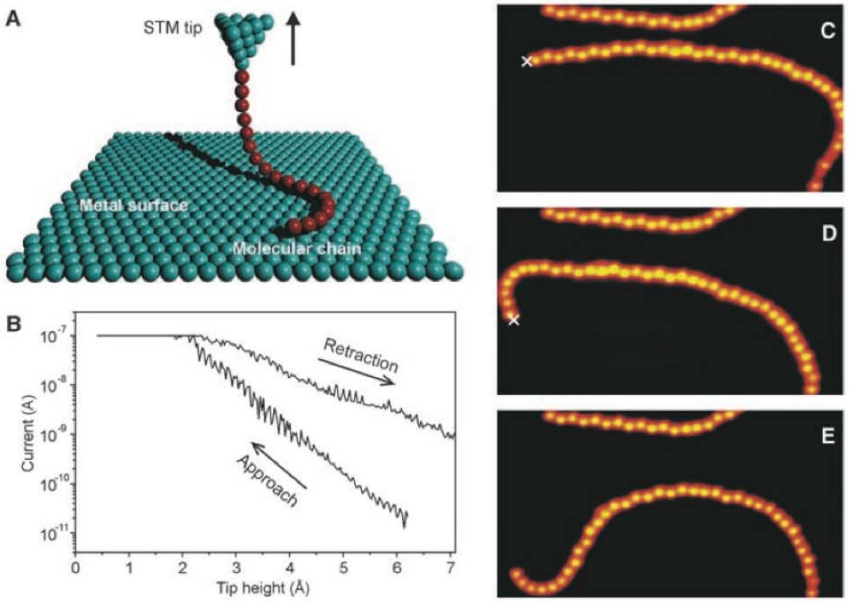

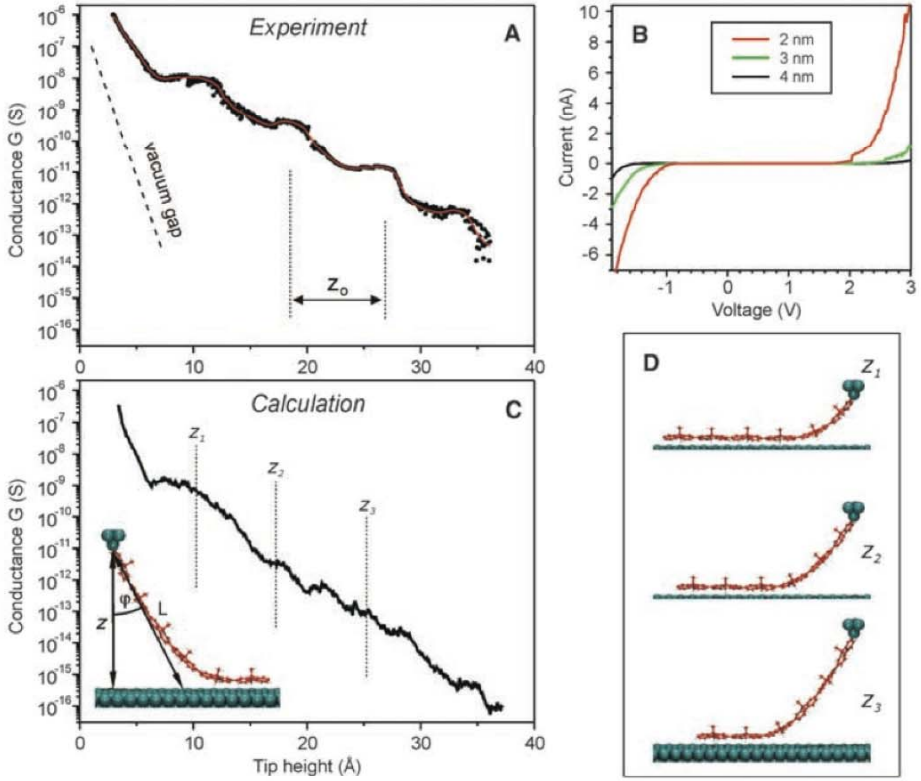

Fig. 3. Conductance as a function of the length of the molecular wire. Experimental (**A**) and calculated (**C**) *G*(*z*) curves (equally scaled), both exhibiting characteristic oscillations with a period of z_o (the decay of a vacuum gap is plotted for comparison). The experimental curve is composed of two data sets from measurements below and above about 20 Å, respectively, using different setups and thus ranges for current detection (each about four orders of magnitude). (**B**) *I-V* curves (of single wires and thus not averaged) at three tip-surface distances (2, 3, and 4 nm). (**D**) Schematic views of characteristic conformations during the pulling process, just before the detachment of another molecular unit (z_1 = 10.2 Å, z_2 = 17.2 Å, and z_3 = 25.2 Å). The inset in (C) shows a sketch with the characteristic parameters *z*, *L*, and φ.

Science, 323, 1193, 2009.

分子にさわったときの振動状態の変化

STM

DOI: 10.1021/nl903760k

Surveying Molecular Vibrations during the Formation of Metal−Molecule Nanocontacts

Lucia Vitali,*,† Robin Ohmann,† and Klaus Kern†,‡

† Institut de
, Switzerland

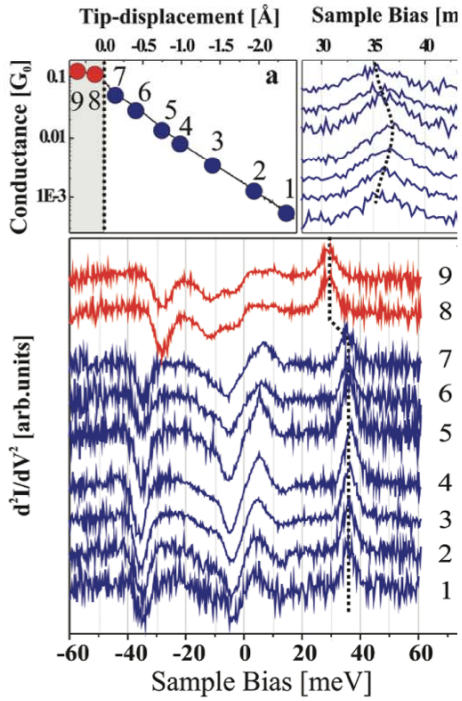

FIGURE 1. Conductance and vibration spectra for individu molecules on a Cu(111) surface at different tip−substrate dis ranging from tunneling to point contact. (a) Variation conductance vs tip displacement. (b) Vibration spectra re using a lock-in amplifier (amplitude of the modulation volta = 2.5 meV) at the positions indicated in (a). The curv normalized to the tunneling current at the correspondi displacement. A vertical offset has been added for a better vis tion. (c) Enlarged section of the spectra reported in (b) show FR mode achieved in tunneling conditions. The dotted lines and (c) highlight the shift of the FR mode vs the tip position

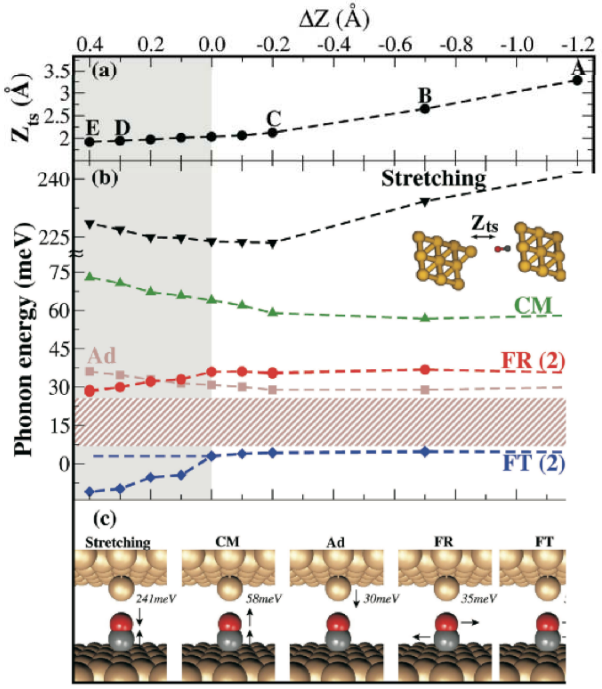

FIGURE 2. (a) Variation of the distance of the tip to the oxygen Z_{ts} with ΔZ showing structural relaxations at the junction. ΔZ is d by the variation in the distance between Cu(111) planes that a relaxed during the approach to contact (second layers of th electrodes). $\Delta Z = 0$ corresponds to the instant of contact formation. (b) Evolution of the CO/Cu(111) vibration modes. Stretching, CM, FR(2), and FT(2) are CO vibration modes, while Ad is the tip−apex Cu adatom longitudinal vibration (see the text). The shaded area covers a region of topmost layer Cu atoms vibrations. At a tip−sample separation of $Z_{ts} \sim 2$ Å a clear change is seen in the vibration energy of the IETS most active FR mode. The geometry of the junction is also schematically shown. (c) Sketch showing the vibration modes.

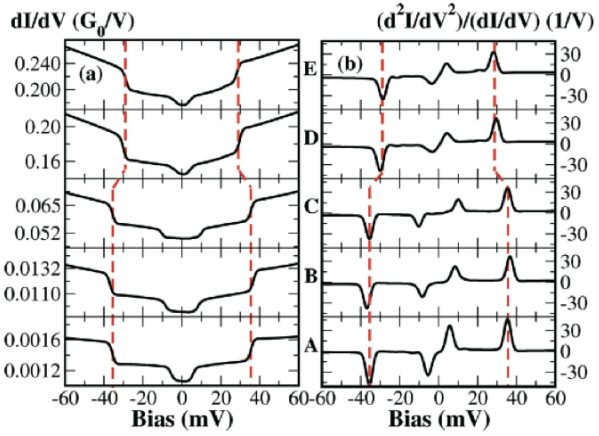

FIGURE 3. Calculated conductance (a) and vibration (b) spectra taken on top of a CO molecule adsorbed on a Cu(111) surface at different tip−sample distances shown in Figure 2. A clear shift (red dotted lines) to lower energies is seen in the FR mode where the peak position shifts from 35 to 29 meV as point contact is approached from tunneling.

輸送特性の制御や分子の持つ機能の発現の例

きわめて安定

MCBJ

Controlled Stability of Molecular Junctions**

*Diana Dulić, Florian Pump, Stephane Campidelli, Pascal Lavie, Gianaurelio Cuniberti, and Arianna Filoramo**

DOI: 10.1002/anie.200902168

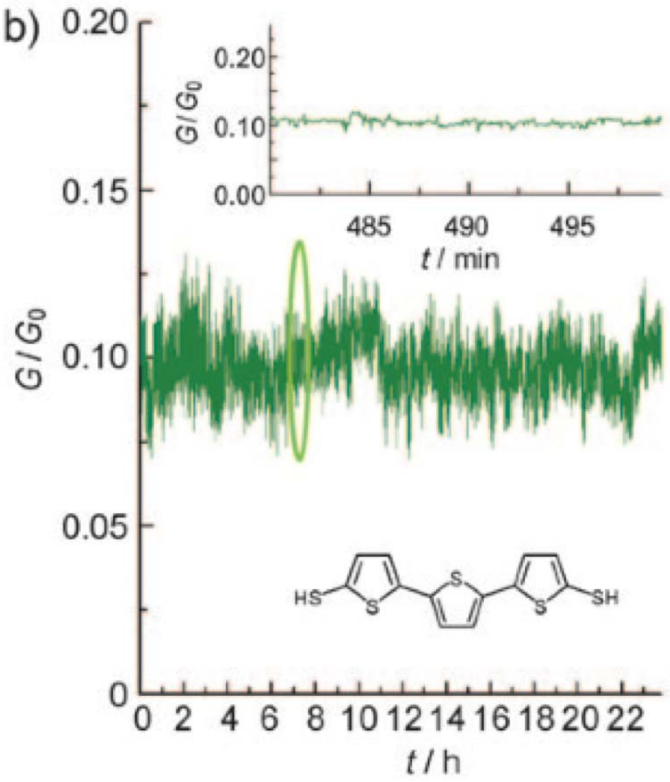

横軸単位：hour

Angew. Chem. 48, 1, 2009.

1 week 安定

期待される輸送特性

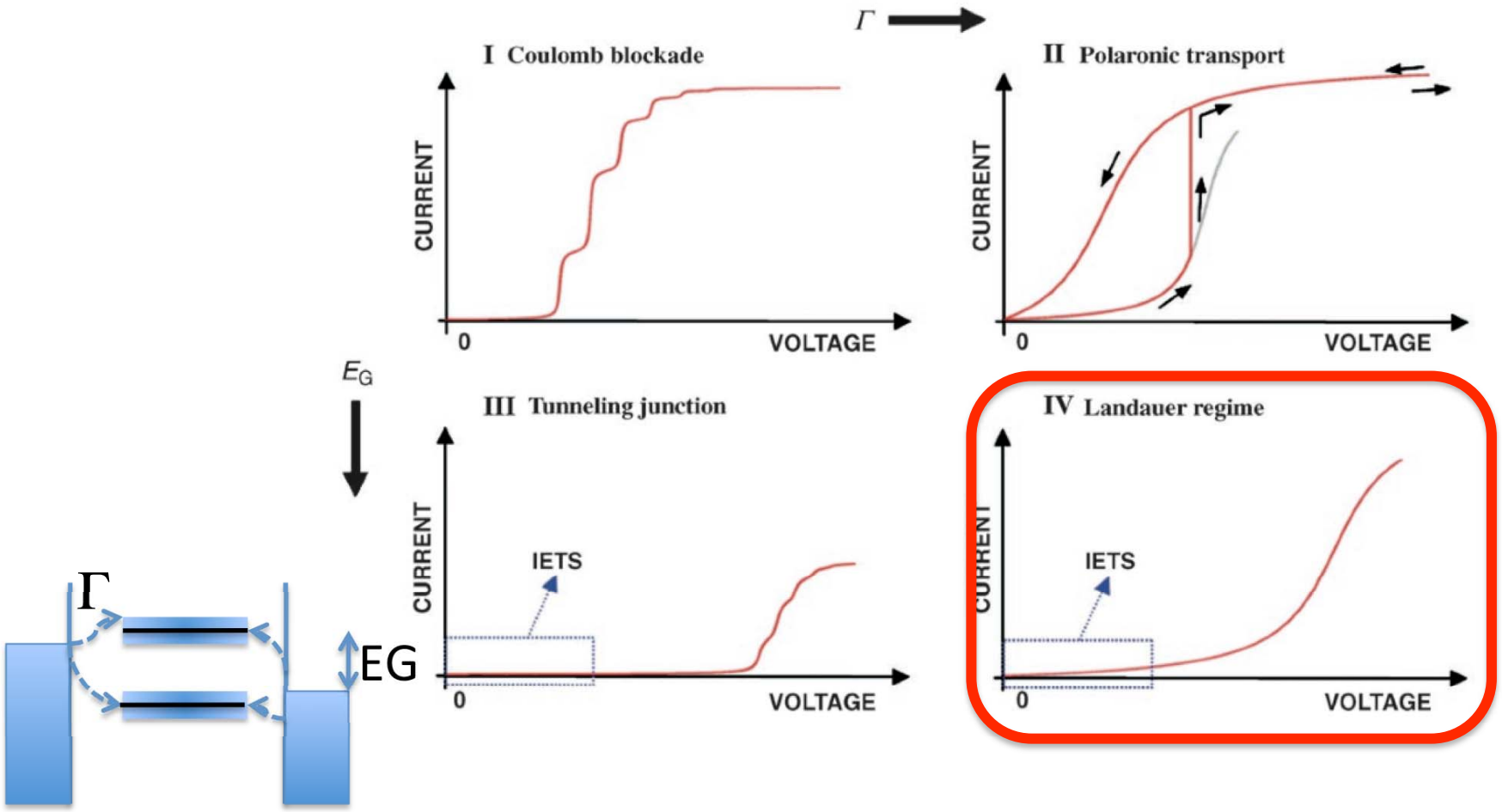

Troisi and Ratner, small, 2, 172, 2006.

高いコンダクタンス

MCBJ

Highly Conductive Molecular Junctions Based on Direct Binding of Benzene to Platinum Electrodes

M. Kiguchi,[1,*] O. Tal,[1] S. Wohlthat,[2,3] F. Pauly,[3] M. Krieger,[1,†] D. Djukic,[1] J. C. Cuevas,[4,3] and J. M. van Ruitenbeek[1]

PRL, 101, 04681,2008.

アンカーを使わずに直接分子を挟む

ベンゼンで ~1G_0

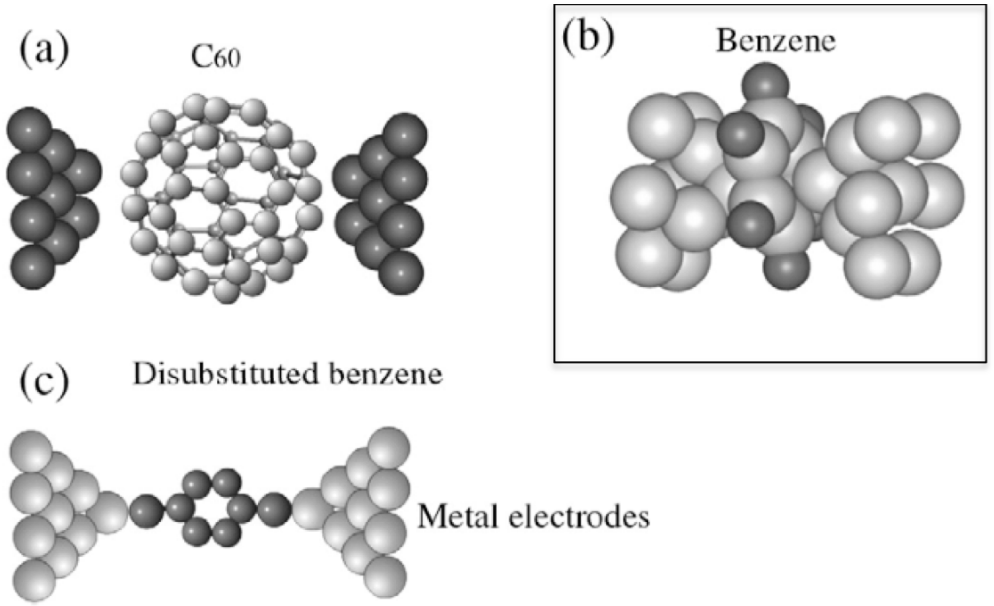

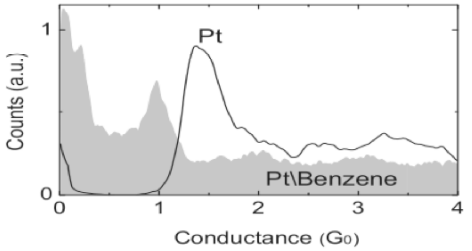

FIG. 1. Conductance histograms (normalized to the area under the curves) for a Pt junction (black), and for Pt after introducing benzene (filled). Each conductance histogram is constructed from more than 3000 conductance traces recorded with a bias of 0.1 V during repeated breaking of the contact.

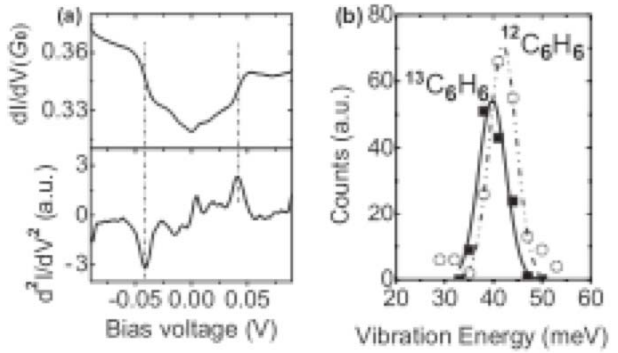

フォトスイッチ

MCBJ

One-Way Optoelectronic Switching of Photochromic Molecules on Gold

Diana Dulić,[1] S. J. van der Molen,[1] T. Kudernac,[2] H. T. Jonkman,[3] J. J. D. de Jong,[2] T. N. Bowden,[2] J. van Esch,[2] B. L. Feringa,[2] and B. J. van Wees[1]

PRL, 91, 207402, 2003.

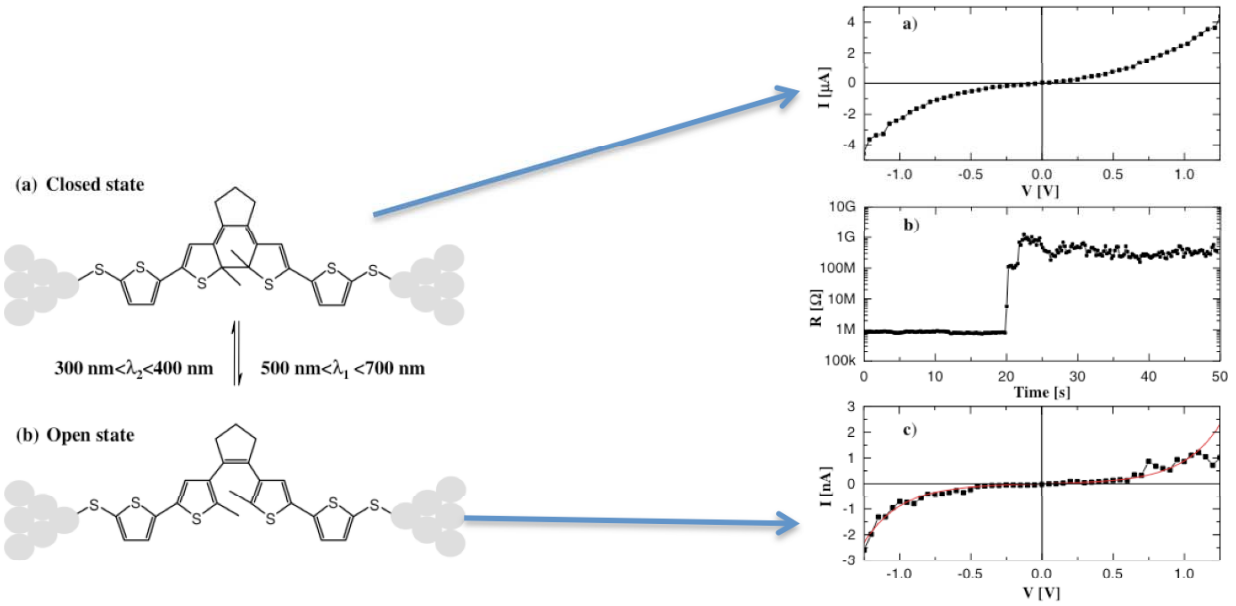

一方通行

FIG. 3 (color online). MCBJ results. (a) Typical IV of the connected molecule in the closed form and (b) resistance versus time. At $t = 0$ a lamp is turned on ($\lambda = 546$ nm). After approximately 20 s a clear jump is observed (1 V bias). (c) Typical IV of the molecule after switching. The line is a fit to the Stratton formula (for details see text).

Nanotechnology, 16, 695, 2005（別グループ）で可逆スイッチが報告

MCBJの弱点

A Nanoelectromechanical Single-Atom Switch

Christian A. Martin,*,†,‡ Roel H. M. Smit,‡ Herre S. J. van der Zant,† and Jan M. van Ruitenbeek‡

NANO LETTERS

2009
Vol. 9, No. 8
2940-2945

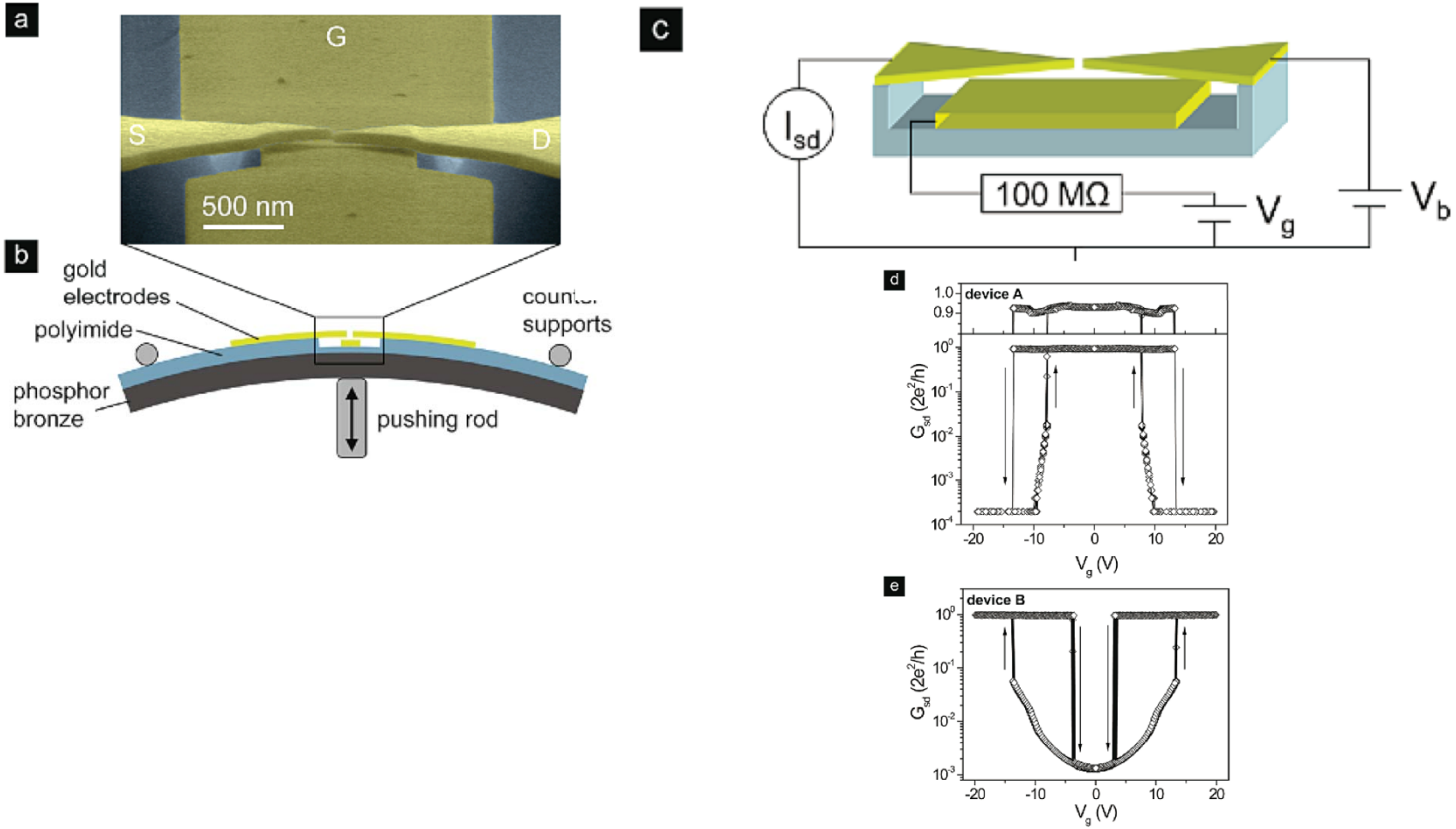

その他の手法をつかって測った例

- エレクトロマイグレーション
- 斜め蒸着

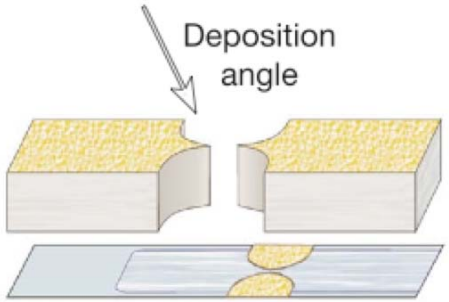

主としてゲート効果をしらべるために利用されている。
分子の数、コンタクト制御に関しては不確定。

分子接合の電気伝導度を決める要因

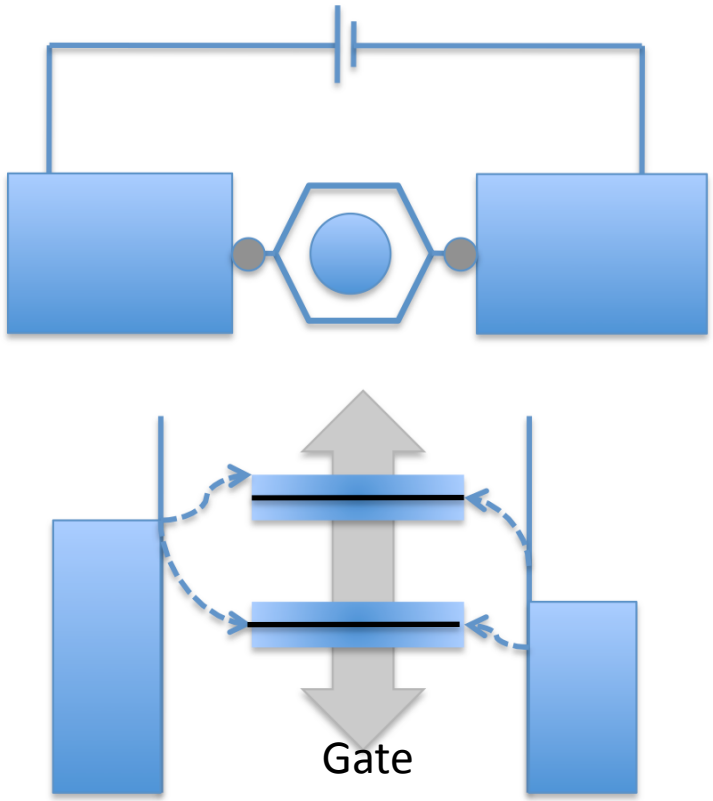

・電極との電子カップリングにより分子軌道が広がる。
・広がりの幅はコンタクト部分の設計により調整可能。

1. 分子の電子状態

2. 分子／電極のカップリングの強さ

電極／分子カップリングの調整

斜め蒸着

Electronic Transport in Single Molecule Junctions: Control of the Molecule-Electrode Coupling through Intramolecular Tunneling Barriers

Andrey Danilov,[†,‡] Sergey Kubatkin,[‡] Sergey Kafanov,[‡] Per Hedegård,[†] Nicolai Stuhr-Hansen,[†] Kasper Moth-Poulsen,[†] and Thomas Bjørnholm*[,†]

Nano Lett. 8, 1, 2008.

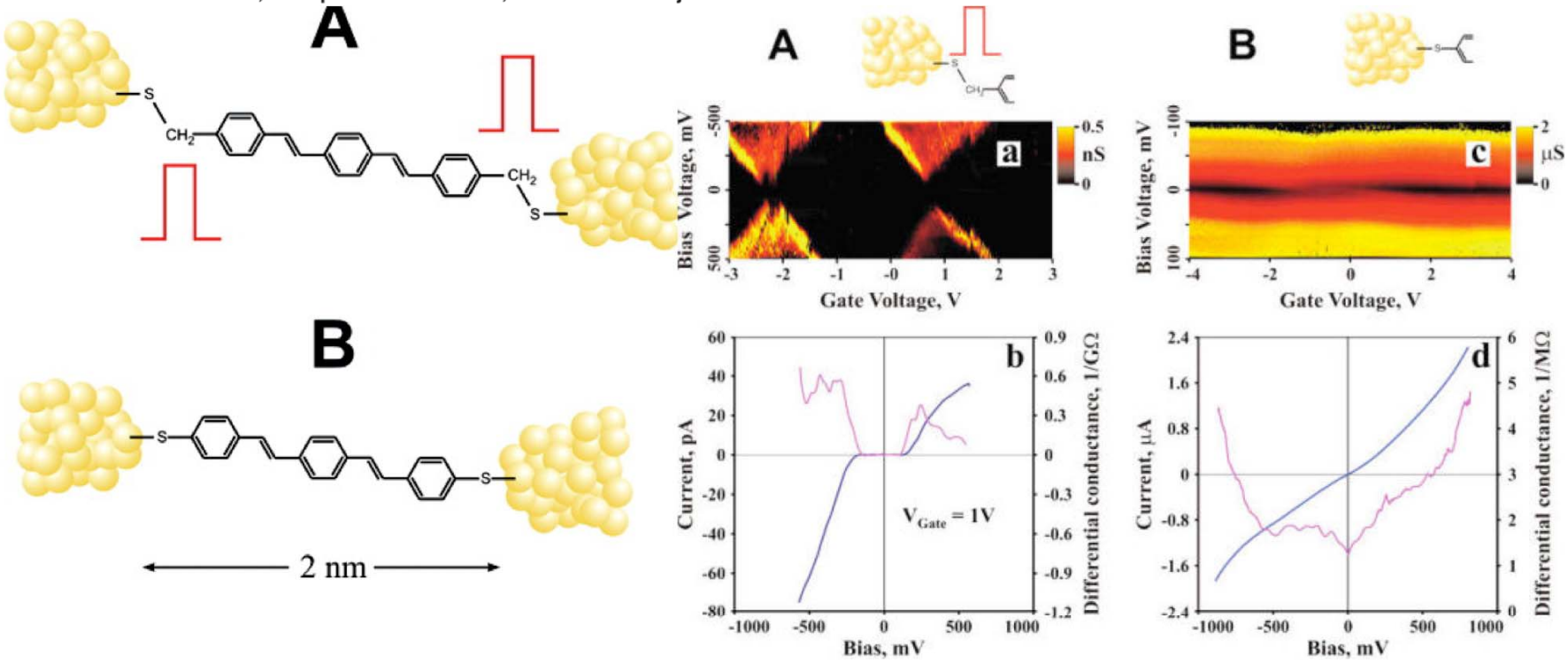

ゲート効果 : Redox stateでクーロンブロッケード

斜め蒸着

Single-electron transistor of a single organic molecule with access to several redox states

Sergey Kubatkin[1], Andrey Danilov[1], Mattias Hjort[2], Jérôme Cornil[2,3], Jean-Luc Brédas[2,3]*, Nicolai Stuhr-Hansen[4], Per Hedegård[4] & Thomas Bjørnholm[4]

Nature, 425, 698, 2003.

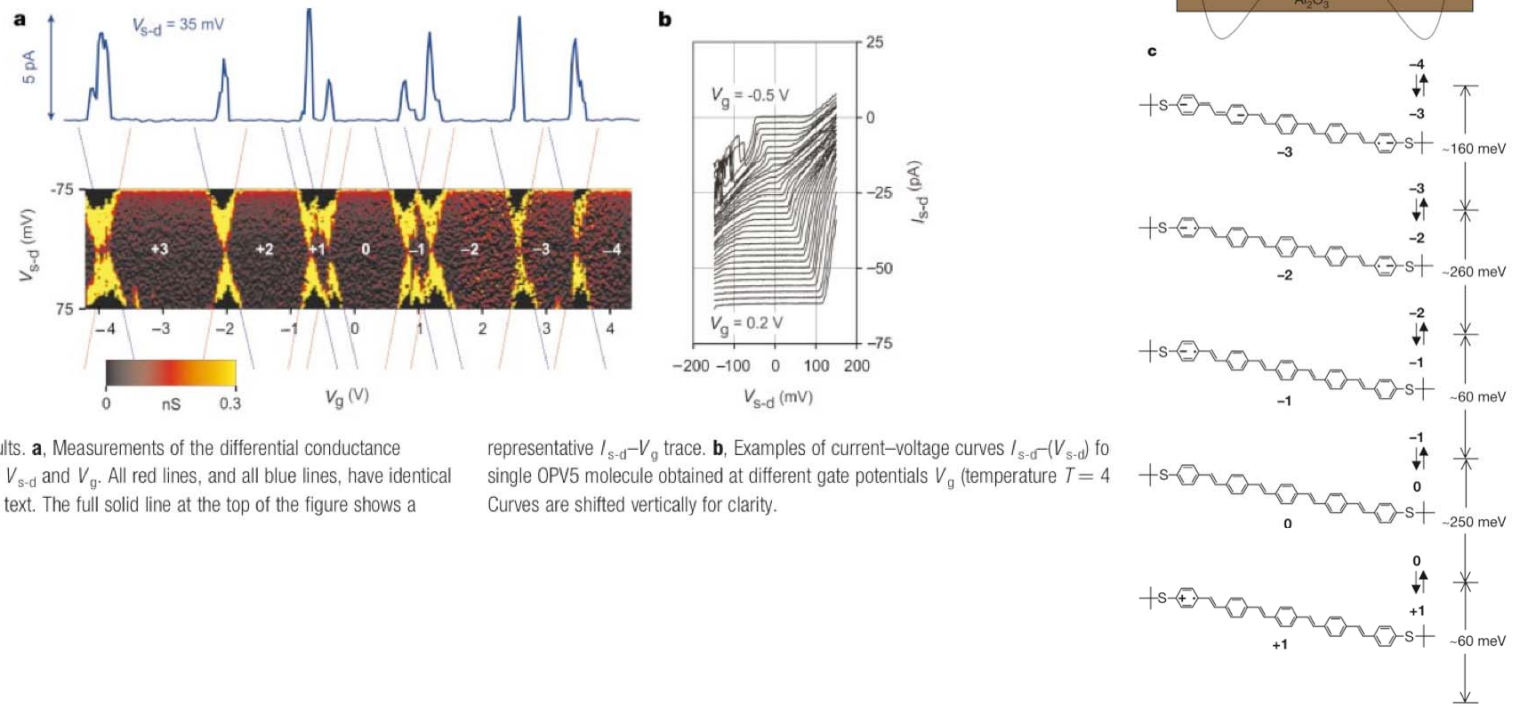

Figure 2 Experimental results. **a**, Measurements of the differential conductance ($dI_{s\text{-}d}/dV_{s\text{-}d}$) as function of $V_{s\text{-}d}$ and V_g. All red lines, and all blue lines, have identical slopes, as discussed in the text. The full solid line at the top of the figure shows a representative $I_{s\text{-}d}$–V_g trace. **b**, Examples of current–voltage curves $I_{s\text{-}d}$–($V_{s\text{-}d}$) fo single OPV5 molecule obtained at different gate potentials V_g (temperature $T = 4$ Curves are shifted vertically for clarity.

ゲート効果

EM

Observation of molecular orbital gating

Nature 462, 1039, 2009.

Hyunwook Song[1,2], Youngsang Kim[3]†, Yun Hee Jang[2], Heejun Jeong[3], Mark A. Reed[4] & Takhee Lee[1,2]

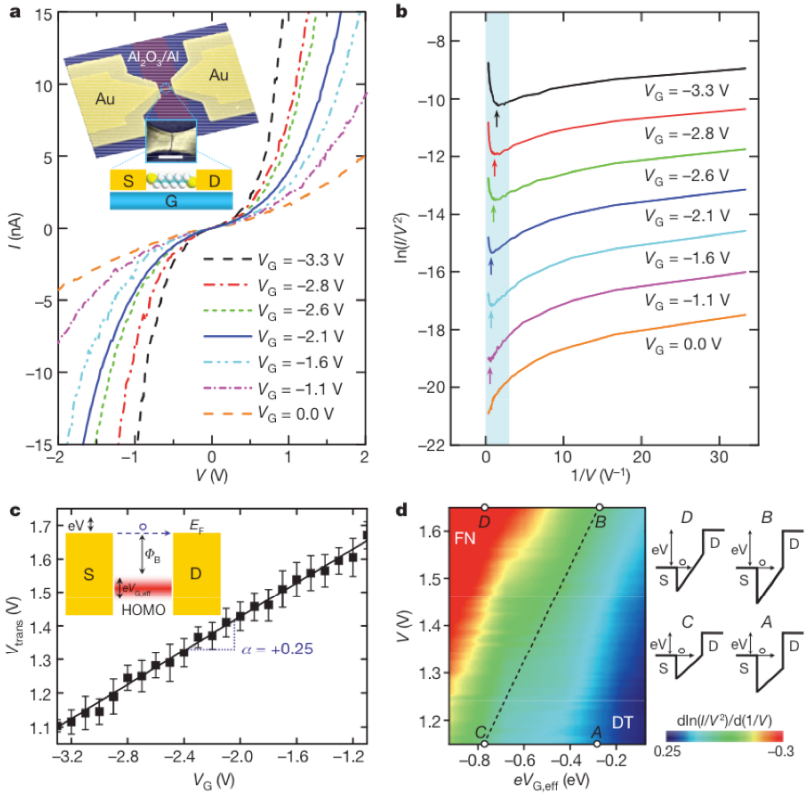

Figure 1 | Gate-controlled charge transport characteristics of a Au-ODT-Au junction. **a**, Representative $I(V)$ curves measured at 4.2 K for different values of V_G. Inset, the device structure and schematic. S, source; D, drain; G, gate. Scale bar, 100 nm. **b**, Fowler–Nordheim plots corresponding to the $I(V)$ curves in **a**, exhibiting the transition from direct to Fowler–Nordheim tunnelling with a clear gate dependence. The plots are offset vertically for clarity. The arrows indicate the boundaries between transport regimes (corresponding to V_{trans}). **c**, Linear scaling of V_{trans} in terms of V_G. The error

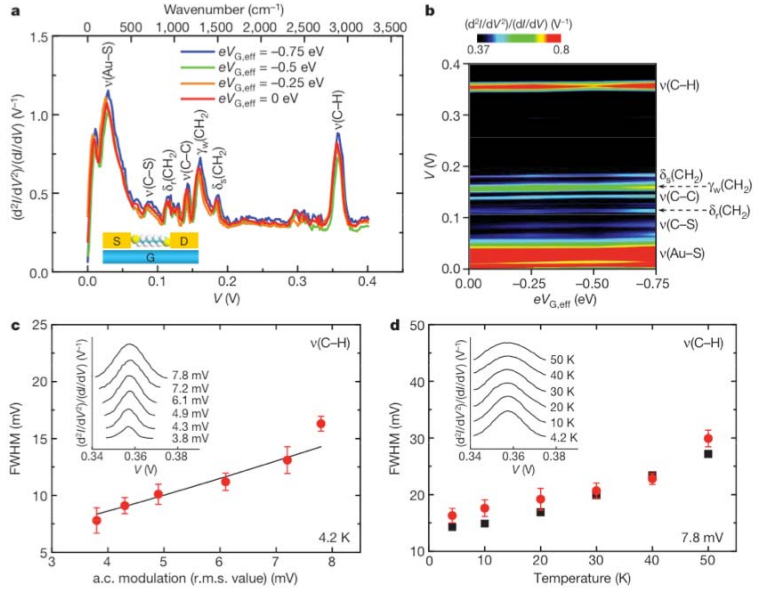

Figure 3 | Gated IET spectra and linewidth broadening of a Au-ODT-Au junction. **a**, IET spectra measured at 4.2 K for different values of $eV_{G,eff}$, with vibration modes assigned. **b**, Two-dimensional colour map of the gated IET spectra, indicating near independence with respect to $eV_{G,eff}$. **c**, **d**, Full-width at half-maximum (FWHM) of the peak corresponding to the ν(C–H) stretching mode (~357 mV) as a function of a.c. modulation voltage (**c**) and

temperature (**d**). The circles indicate experimental data, and the solid line (**c**) and squares (**d**) show theoretical values. The error bars are determined by the Gaussian fitting. Insets, successive IET spectroscopy scans for the ν(C–H) mode under increasing a.c. modulation voltage (**c**) and increasing temperature (**d**), as indicated. r.m.s., root mean squared.

Nature 462, 1039, 2009.

前ページより続く

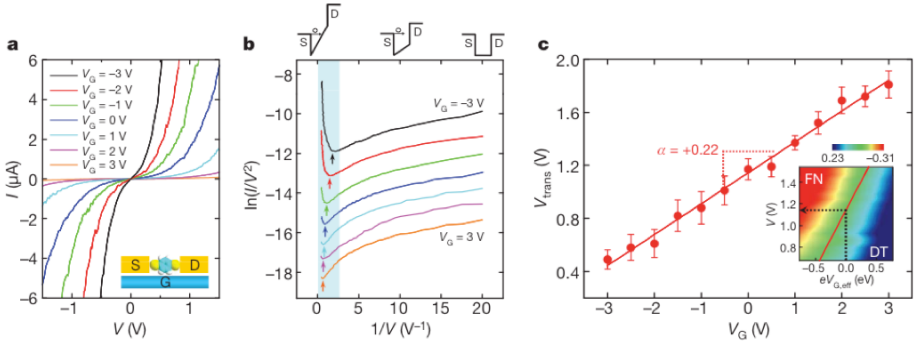

Figure 2 | Gate-controlled charge transport characteristics of a Au-BDT-Au junction. **a**, Representative $I(V)$ curves measured at 4.2 K for different values of V_G. **b**, Fowler–Nordheim plots demonstrating the gate-variable transition from direct to Fowler–Nordheim tunnelling (colour-coded as in **a**). The plots are offset vertically for clarity. Also shown are drawings of the barrier shape with increasing bias. **c**, Plot of V_{trans} versus V_G. The solid line is a linear fit and the error bars denote the s.d. of the individual measurements. Inset, the colour map of $d\ln(I/V^2)/d(1/V)$ (from Fowler–Nordheim plots) with linear fit (solid line) obtained from the plot of V_{trans} versus V_G. The zero-gate transition voltage is indicated by the dashed arrow.

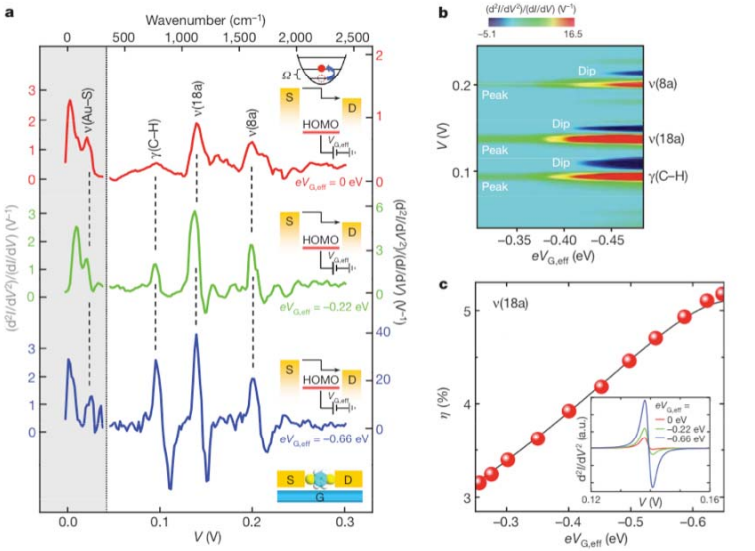

Figure 4 | Resonantly enhanced IET spectra of a Au-BDT-Au junction. **a**, IET spectra measured at 4.2 K for different values of $eV_{G,eff}$, with vibration modes assigned. The left-hand y axis corresponds to the grey shaded region of the spectra, and the various right-hand y axes (with different scales) correspond to the related (colour-coded) spectra in the non-shaded region. The vertical dotted line corresponds to $V = 45$ mV (363 cm^{-1}). Significant modification in the spectral intensity and line shape for the benzene ring modes, γ(C–H), ν(18a) and ν(8a), was observed for different values of $eV_{G,eff}$, as indicated. Insets, energy diagrams illustrating inelastic tunnelling as the position of the HOMO resonance shifts as a result of gating. **b**, Two-dimensional colour map of the gated IET spectra, showing that IET spectroscopy intensity and line shape vary significantly as functions of $eV_{G,eff}$. **c**, The relative change, η, in the normalized conductance for the ν(18a) mode as a function of $eV_{G,eff}$. The circles show the experimental data and the solid curve represents the theoretical fit calculated from equation (1). Inset, the gate-variable IET spectra for the ν(18a) mode, simulated using equation (1). a.u., arbitrary units.

磁気抵抗効果

EM

The Kondo Effect in the Presence of Ferromagnetism

Abhay N. Pasupathy,[1] Radoslaw C. Bialczak,[1] Jan Martinek,[2]
Jacob E. Grose,[1] Luke A. K. Donev,[1] Paul L. McEuen,[1]
Daniel C. Ralph[1]*

Science, 306, 86, 2004.

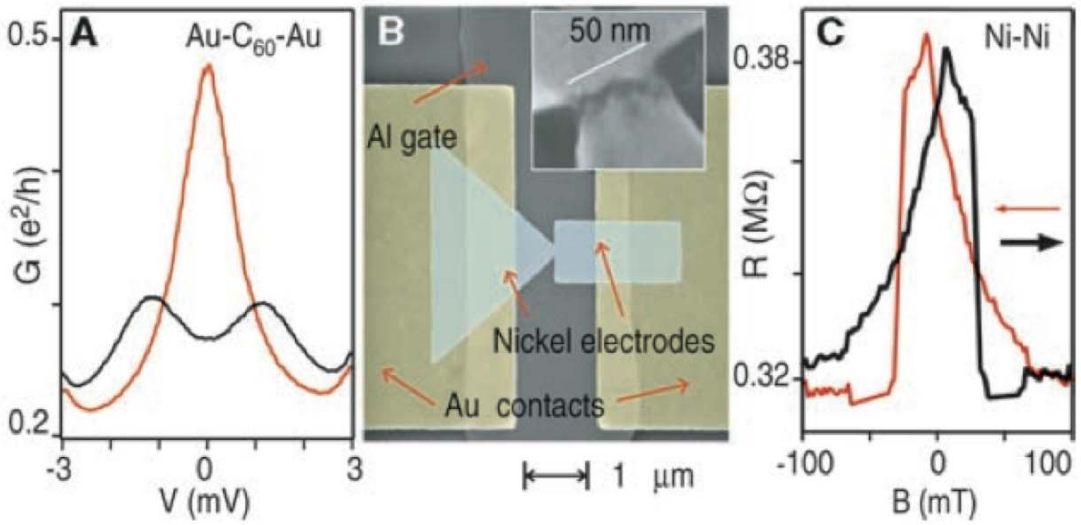

Fig. 1. (**A**) Kondo signal for C_{60} with Au electrodes at T = 1.5 K. At B = 0 (red line), there is a zero-bias peak in $G(V)$ that becomes split for B = 10 T (black line). (**B**) Scanning electron micrograph of a Ni break junction. The magnetic field is applied in the horizontal direction. (**Inset**) Close-up of the junction region after electromigration. (**C**) Tunneling magnetoresistance near V = 0 at T = 4.2 K of a Ni contact after electromigration, with no C_{60} molecule present.

エレクトロマイグレーション

可逆抵抗スイッチ

EM

Reversible and Controllable Switching of a Single-Molecule Junction**

*Emanuel Lörtscher, Jacob W. Ciszek, James Tour, and Heike Riel**

small, 2, 973, 2006.

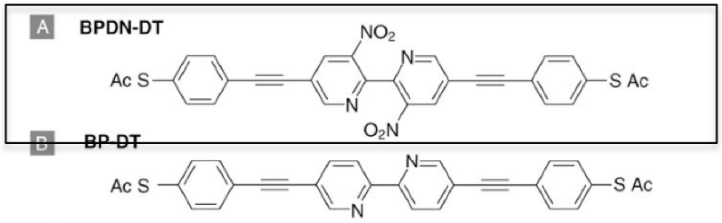

Aはスイッチ挙動を起こし、Bは起こさない。

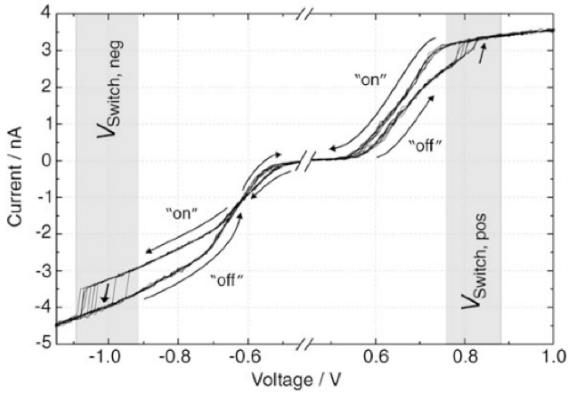

Figure 3. Several repeated switching cycles of the BPDN-DT: If the voltage applied to the metal–BPDN-DT–metal junction exceeds a certain positive threshold value ($V_{Switch,pos}$), the system switches from the initial "off" state to the "on" state. This state is maintained when operating only at voltages above $V_{Switch,pos}$. A negative voltage sweep or a pulse below the negative threshold value ($V_{Switch,neg}$) resets the molecule again to the initial "off" state.

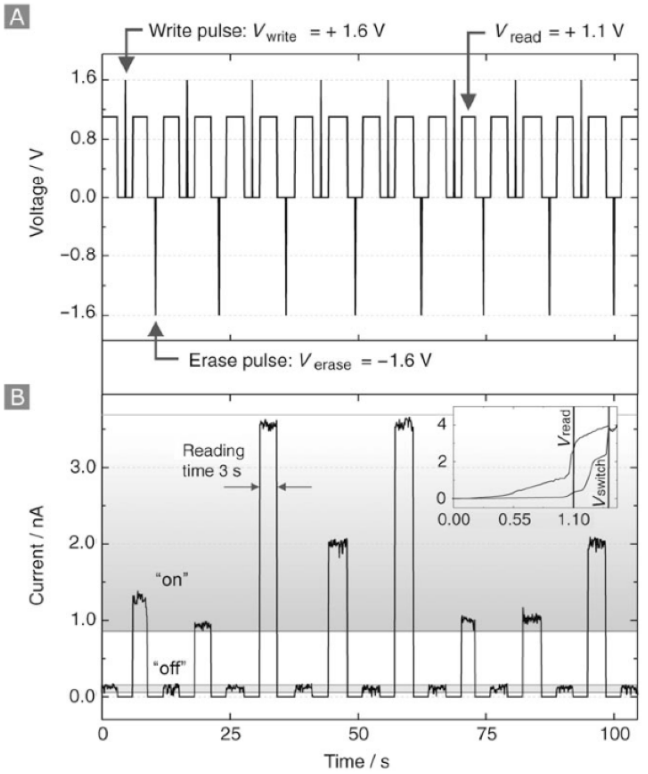

Figure 5. Memory operation of the BPDN-DT system: A) Write, read, and erase voltage pulse pattern applied. B) Resulting switching between "off" and "on" state: I_{off} varies between 0.05 and 0.13 nA, I_{on} between 0.9 and 3.6 nA. Reading times of 3 s display excellent signal stability. The inset shows the corresponding *I–V* curve, indicating switching at 1.4 V and reading at 1.1 V (black lines).

おおざっぱな現状の位置づけ

- ☑単分子の電気抵抗を測れるか？
- ☑定性的な伝導特性の解釈はできるか？
- □定量的な解釈はできるか？
- ☑外部変調は可能か？
- ☑整流特性は出るか？
- ☑分子の個性／機能は出せるか？

- □つかえるか？

Oligoaryl Cruciform Structures as Model Compounds for Coordination-Induced Single-Molecule Switches

Sergio Grunder,[a] Roman Huber,[b] Songmei Wu,[b] Christian Schönenberger,[b] Michel Calame,*[b] and Marcel Mayor*[a,c]

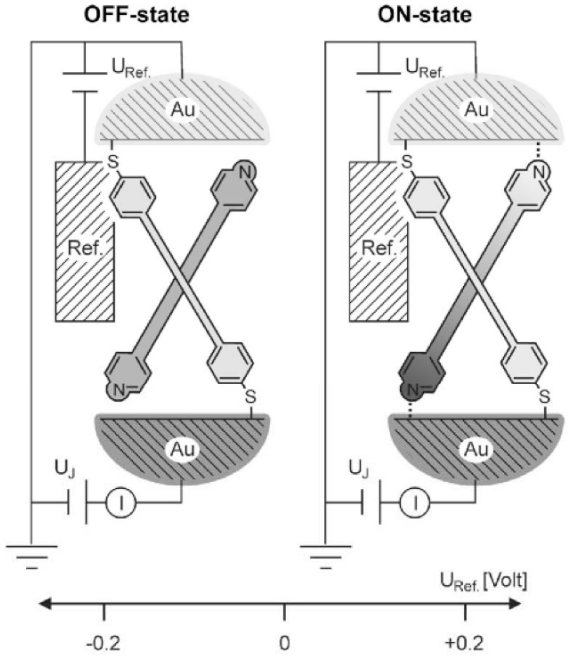

Figure 1. Coordination-induced switching principle: the coordination of the better conducting terminally pyridine-functionalized bar subunit to both electrodes is controlled by the electrochemical potential applied with respect to a reference electrode. Upon coordination (ON-state) the potential between both electrodes triggers electron transport through the bar subunit.

Eur. J. Org. Chem. **2010**, 833–845

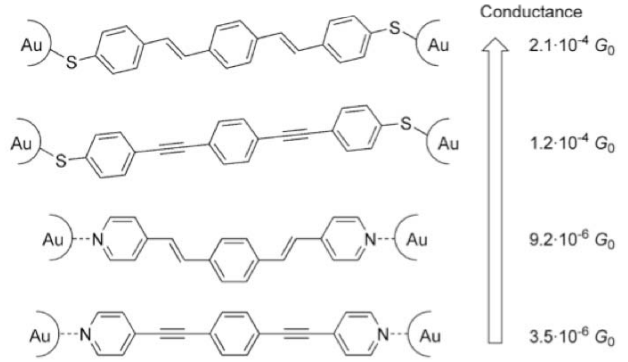

Figure 2. Measured trend in the conductivity of the OPV and OPE rods with terminal sulfur or pyridine anchor groups.

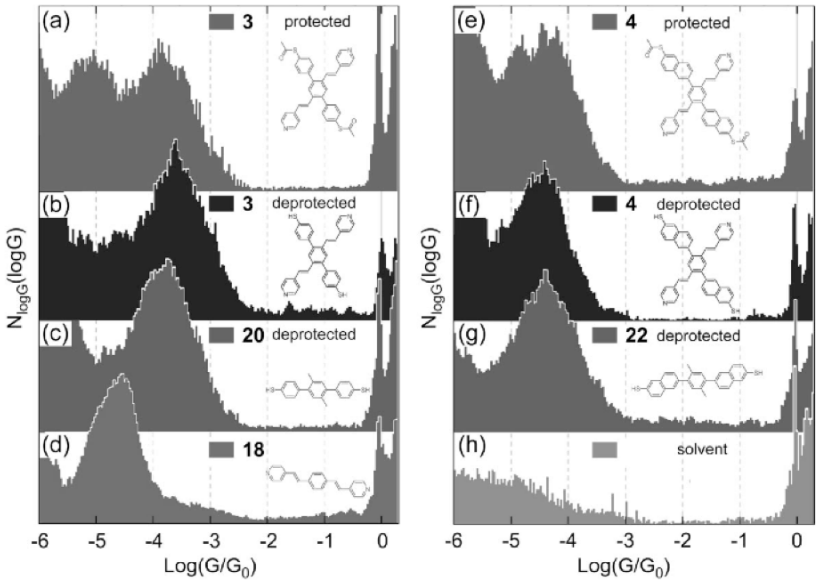

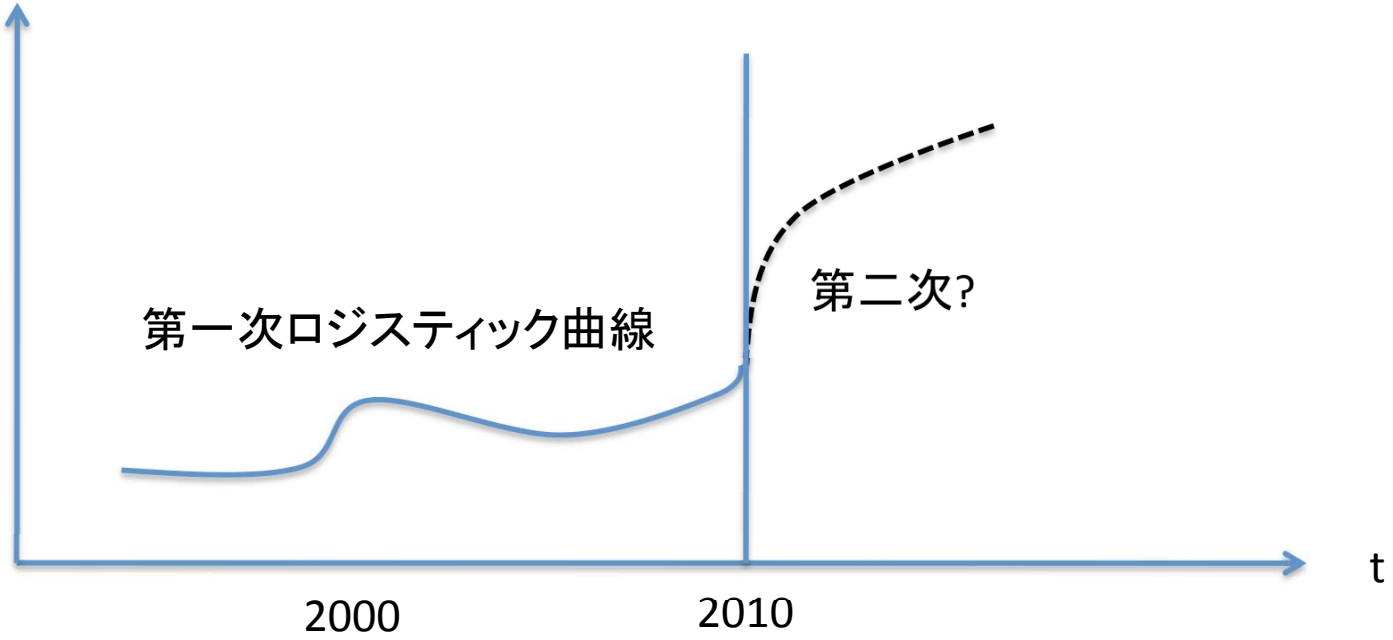
第一次ロジスティック曲線
第二次?
t
2000
2010

ゲート電圧によるスピン状態の制御

斜め蒸着

Electrical Manipulation of Spin States in a Single Electrostatically Gated Transition-Metal Complex

Edgar A. Osorio,[†] Kasper Moth-Poulsen,[†] Herre S. J. van der Zant,*[,†] Jens Paaske,[†] Per Hedegård,[†] Karsten Flensberg,[†] Jesper Bendix,[†] and Thomas Bjørnholm[†]

DOI: 10.1021/nl9029785

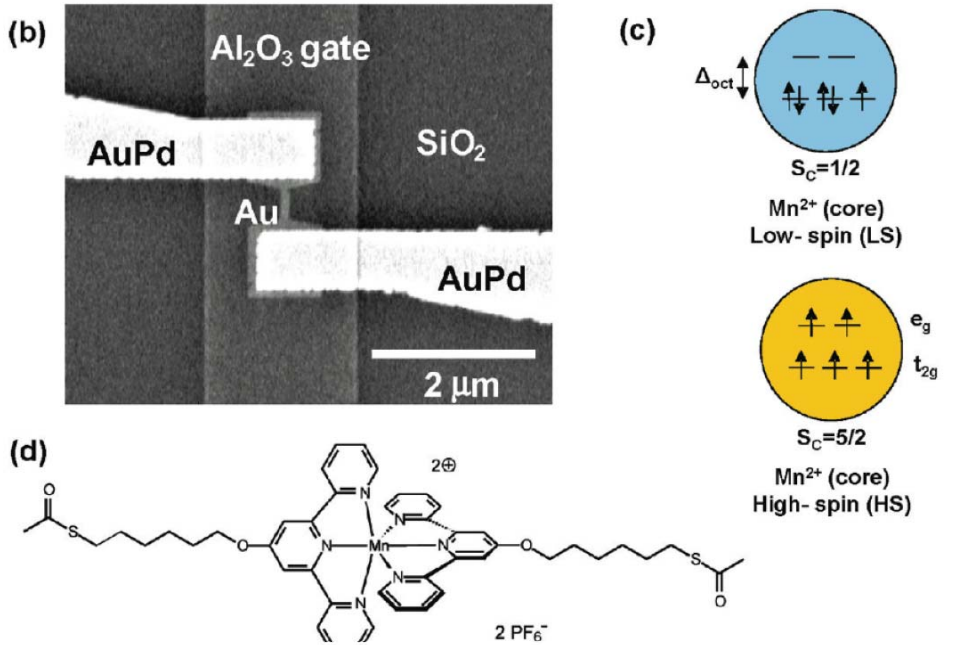

FIGURE 1. (a) Schematic device lay-out and artistic impression of a ([Mn(terpy-O-$(CH_2)_6$-SAc$_2$)]$^{2+}$) molecule bo The asymmetric geometry illustrates a likely realization of the device which gives rise to asymmetric coupling to and the difference in gate-coupling to the two ligand moieties that is implied by our transport data. (b) Fabric the small gold wire in the middle by electromigration. The junction is fabricated on top of an aluminum gate el air to form a 2−4 nm thick Al_2O_3 layer, and at low temperatures substantial leakage currents are typically obse Bridges are electromigrated in the molecule solution at room temperature by ramping a voltage until a decrease in upon which the applied voltage is returned to 100 mV; the cycle is repeated until a target resistance of electromigrated bridges are then left in the molecule solution for about one hour to allow for molecular self-ass the constricted gold wire. Last, the sample space is evacuated and the cooling procedure to 1.7 K starts. (c) configurations of the Mn^{2+} core with respectively low, and high spin are given. The d-orbitals on the Mn atom are s ligand field of the organic terpyridine cage into three (lower) t_{2g} orbitals and two (upper) e_g orbitals. (d) Molec O-$(CH_2)_6$-SAc$_2$)]$^{2+}$). The derivative has CH_6 alkane chains attached to the ligands and acetyl protected thiol en with the gold electrodes.

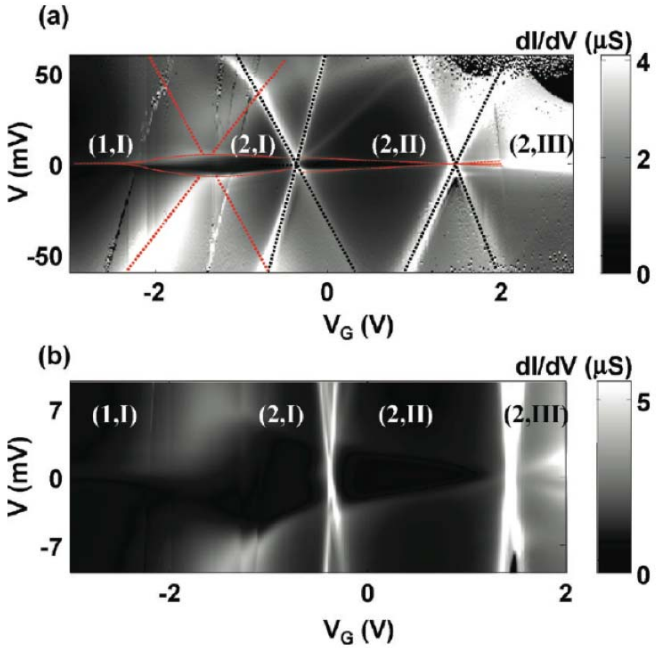

FIGURE 2. (a) Density plot of the differential conductance, dI/dV, versus V and V_G at T = 1.7 K. The different charge states of respectively the main molecule and the molecule in parallel are indicated by (i,j) with i = 1,2 and j = I, II, III. The molecule in parallel gives rise to two very similar white crosses of high conductance due to sequential tunnelling (black dotted lines). The main molecule displays only a single cross (red dotted lines) corresponding to sequential tunnelling, which is strongly perturbed due to its very strong coupling to one, but not the other electrode, and due to the spin-blockade hindering ground state to ground state transport at low-bias. Solid red lines trace out the inelastic cotunneling edges due to virtual tunnelling processes in and out of charge state (2). Black areas at the top right of the figure are due to saturation of the current amplifier. (b) Low bias zoom-in of the different crossings and charge states without any guides to the eye.

前ページより続く

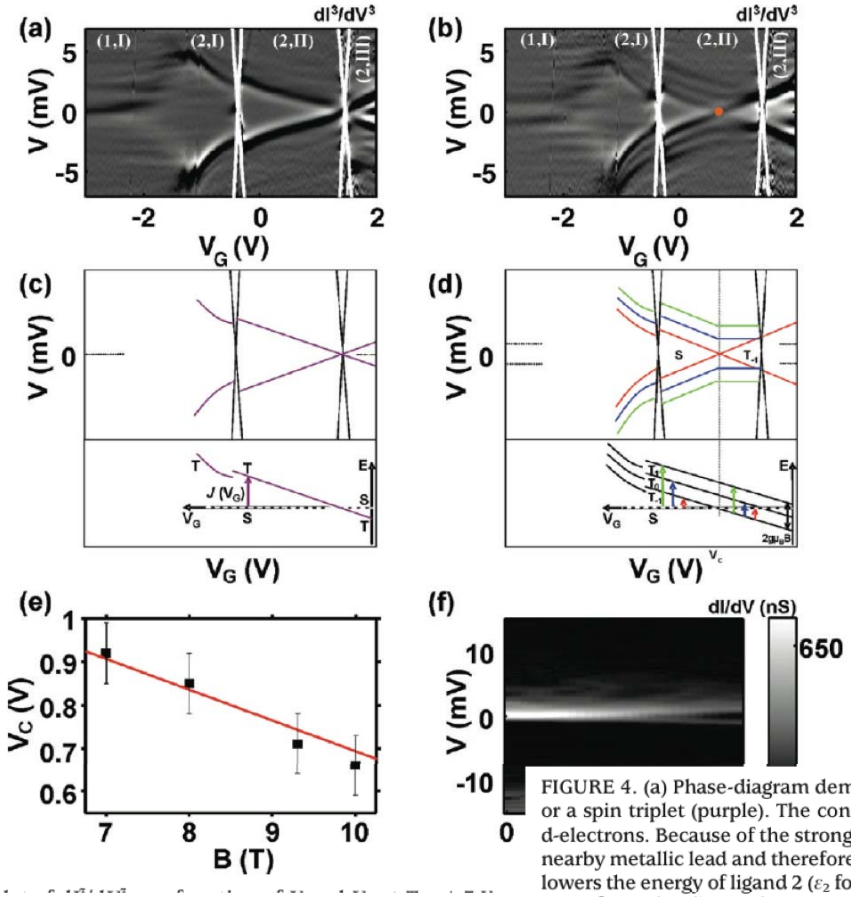

FIGURE 3. (a) Gray scale plot of dI^3/dV^3 as a function of V and V of the dI/dV which was measured with a lock-in technique. W low-bias features; resonances in the first derivative appear as d superimposed on the plot at the diamond edge locations as a gr the important low bias features observed in (a); (bottom) energ in charge state (2). The energy splitting between S and T is giver of (b); (bottom) energy diagram with Zeeman splitting of the triplet states. Arrows indicate all observed transitions in charge state (2, I−III). The vertical dashed line locates the S-T_{-1} crossing; as indicated on the top part, the singlet (triplet) is the ground state at the left (right) side of this line. (e) Squares: gate voltage value of the S−T_{-1} crossing, V_C, for four different magnetic fields. Red line gives the predicted gate voltages of the S−T_{-1} crossing, using the energy diagram presented in (d), as a function of magnetic field. (f) Gray scale plot of dI/dV vs B-field showing a Zeeman splitting of the Kondo resonance at $V_g = -2.8$ V. From the splitting at $B = 10$ T, we estimate a g-factor of $g = 1.9 \pm 0.3$.

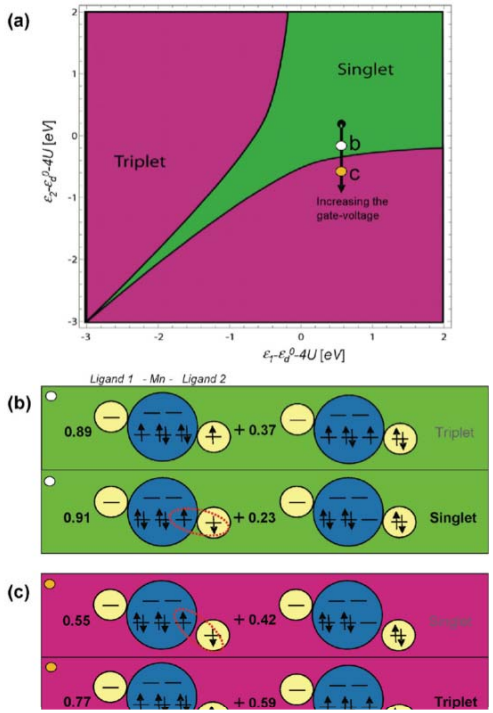

FIGURE 4. (a) Phase-diagram demarcating the regions for which the ground state of the $N = 6$ electron system is respectively a spin singlet (green) or a spin triplet (purple). The control parameters on the axes represent the energy levels of the relevant ligand states that hybridize with the Mn d-electrons. Because of the strongly asymmetric device geometry, all but the terpyridine moiety lying away from the leads will be screened by the nearby metallic lead and therefore the ligand level of this central terpyridine (ligand 2) feels the gate potential more strongly. Increasing V_g therefore lowers the energy of ligand 2 (ε_2 following the black arrow) and the ground state eventually changes from singlet to triplet as observed when moving away from the diagonal ($\varepsilon_1 = \varepsilon_2$) in Figure 3a,b. (b) The phase diagram in (a) is calculated from an exact diagonalization that reveals a simple understanding in terms of the 6-particle states shown here. Upper (lower) state is a spin singlet (triplet) and the singlet is the ground state at the point in parameter space corresponding to the white dot in panel (a). (c) Same as (b), except that ε_2 has now been moved down to the location of the orange dot in panel (a) and the triplet has become the ground state. As indicated by their numerical coefficients, these states dominate the exact eigenstates and they allow for a simple interpretation of the cause of the gate-dependent singlet−triplet splitting: Basically the triplet is stabilized by charge fluctuations between the d, and the ligand orbitals since it gains more from the Hund's rule coupling on the Mn-core (cf. Section S6 of the Supporting Information for more details). Increasing the gate-voltage lowers ε_2 and, as reflected in the different numerical coefficients, more weight is put on the component with a doubly charged ligand 2, that is, the component where the triplet is lowered more in energy from Hund's rule coupling. Parameters for this plot were chosen to be $U = 5.0$, $\varepsilon_d{}^0 + 4U = 0$, $K = 0.8$, $\Delta = 2.0$, $t = 0.26$ and $t' = 0.1$, all in units of eV.